Western&Graduate&PostdoctoralStudies

3-28-2023 10:00 AM

Depth-Dependent Analysis of Human Ocular Dominance Columns using fMRI with Phase Regression

Brett T. Liem, *The University of Western Ontario*

Supervisor: Menon, Ravi S., *The University of Western Ontario*
A thesis submitted in partial fulfillment of the requirements for the Master of Science degree in Medical Biophysics
© Brett T. Liem 2023

Abstract

High-resolution fMRI using gradient-echo blood-oxygen-level-dependent (BOLD) contrast is beneficial for the non-invasive study of neural microcircuits. However, the signal spatial specificity of the BOLD contrast severely limits the ability to localize regions of neural activity at the mesoscopic scale in the cortex due to signal contamination from large veins. Phase regression is a venous bias correction technique that uses the correlation between magnitude and phase data in large veins to estimate and supress their contribution to the BOLD signal. This thesis further investigates the performance of phase regression by examining the laminar BOLD signal in human ocular dominance columns. Phase regression removes the venous bias from pial veins and large intracortical veins, while not removing the venous bias from venous vessel sizes within the cortex running parallel to the cortical surface. This thesis demonstrates improved laminar BOLD signal specificity that will be beneficial in future high-resolution laminar fMRI studies.

Keywords

Summary for Lay Audience

Functional MRI is a popular non-invasive imaging modality that relies on changes in the concentration of blood oxygenation to map changes in neural activity associated with brain function. Neural activity is energy intensive and requires oxygen, leading to changes in local blood oxygenation in areas of neural activity. A major problem with this technique is that blood oxygenation changes are most prominent in large veins because blood drains away from many small vessels in activated regions and pools in fewer large veins. Large veins are more distant from the activated regions, meaning that they are not an accurate measure of blood oxygenation changes caused at the actual site of neural activity.

One technique that attempts to remove the venous bias from the signal is called phase regression and it relies on phase data. MRI acquisitions result in complex-valued data, which is commonly represented as magnitude and phase images, with the phase data typically being discarded. In phase regression, the phase data is used to estimate and suppress the venous bias from the signal. This helps ensure the measured signal is more spatially specific to the site of neural activity.

A laminar and columnar analysis was performed in ocular dominance columns in the human primary visual cortex to investigate the performance of phase regression for high-resolution functional MRI. Ocular dominance columns are vertical columns across the cortex with alternating sensitivity to right and left eyes. They also contain varying amounts of signal exchange between columns at different cortical depths (laminae). This makes ocular dominance columns well suited for performing a laminar and columnar analysis assessment as they are a cortical structure with relatively well-known mesoscopic functions.

It was shown that laminar signal profiles across cortical depths were improved by phase regression. However, phase regression did not help clearly define ocular dominance columns. This is convincing evidence that phase regression is only effective for the largest veins, and not smaller venous vessels within the cortex running parallel to the cortical surface. Overall, this thesis demonstrates that phase regression will be a useful tool for high-resolution functional MRI studies performing laminar analyses.

Co-Authorship Statement

The following thesis is presented in Integrated Article format and contains one unpublished manuscript.

Chapter 2: Liem B. T., Akbari A., Gati J. S., Zeman P., & Menon R. S. Depth-Dependent Analysis of Human Ocular Dominance Columns using BOLD fMRI with Phase Regression at 7 T. In preparation.

Brett T. Liem performed study design conceptualization, software development, guidance on hardware development, participant recruitment, data acquisition, data analysis, data interpretation, drafting the manuscript, as well as manuscript revisions. Atena Akbari provided support on data analysis and data interpretation, as well as proving manuscript revisions. Joseph S. Gati provided guidance on data acquisition and data analysis. Peter Zeman contributed by performing hardware development. Ravi S. Menon provided supervision, study design conceptualization, guidance on software development and data interpretation, as well as manuscript revisions.

Acknowledgments

To my supervisor, Ravi Menon: Thank you for support and guidance throughout my time as a member of your lab. I am extremely grateful for the opportunity and resources you provided that have allowed me to engage in research projects I never truly believed I could be part of. Thank you for continuing to push me to grow not only as a researcher, but as a person.

To the members of my advisory committee: Thank you Ali Khan and Jody Culham for your support and advice throughout my degree. Your knowledge and experience played a big role in many of my important research decisions.

To everyone at the Centre for Functional and Metabolic Mapping (CFMM): Thank you everyone for your endless support, providing such a superb research environment, and making my time here so enjoyable. I would like to extend this thank you to Trevor Szekeres for your assistance with data acquisition, Joe Gati for your expertise with sequence refinement, and Peter Zeman for your work on crucial hardware for my research. I would like to give a special thank you to all the participants who took time out of their day to volunteer for my study, your generosity helped make this research possible.

To my past and present fellow lab members: Thank you for answering my many questions, no matter how frequent those questions were. A big thank you to Olivia Stanley and Atena Akbari who helped guide me throughout my time with phase regression and laminar fMRI research. You were both so thorough when providing me with assistance and helped me more than you probably even realize.

To my friends: Thank you for keeping me sane throughout the ups and downs of research. You provided me a reliable outlet whenever I was feeling stressed and all I needed was to take a step back and relax.

Finally, to my family: Thank you for always being there when I needed support at any hour of the day. You always knew how to reassure me when I was doubting myself and I would not have been able to do this without you.

Table of Contents

List of Figures

List of Abbreviations

BOLD   Blood-Oxygen-Level-Dependent

CBF   Cerebral Blood Flow

CBV   Cerebral Blood Volume

CSF   Cerebrospinal Fluid

DAQ   Data Acquisition

EPI   Echo-Planar Imaging

FA   Flip Angle

FE   Frequency-Encoding

fMRI   Functional Magnetic Resonance Imaging

GE-EPI   Gradient-Echo Echo-Planar Imaging

GLM   General Linear Model

GM   Grey Matter

GRAPPA   GeneRalized Autocalibrating Partially Parallel Acquisitions

GRE   Gradient-Echo

HRF   Hemodynamic Response Function

MP2RAGE   Magnetization Prepared 2 Rapid Acquisition Gradient Echoes

MR   Magnetic Resonance

MRI   Magnetic Resonance Imaging

NORDIC   NOise Reduction with DIstribution Corrected

ODCs	Ocular Dominance Columns
PE	Phase-Encoding
PLATO	Portable Liquid crystal Apparatus for Tachistoscopic Occlusion
RF	Radiofrequency
ROI	Region-of-Interest
ROMEO	Rapid Opensource Minimum spanning treE algOrithm
SAR	Specific Absorption Rate
SE	Spin-Echo
SE-EPI	Spin-Echo Echo-Planar Imaging
SNR	Signal-to-Noise Ratio
SS	Slice-Selective
SVD	Singular Value Decomposition
T1	Longitudinal Relaxation Time
T2	Transverse Relaxation Time
T2*	Apparent Transverse Relaxation Time
TE	Echo Time
TR	Repetition Time
tSNR	Temporal Signal-to-Noise Ratio
V1	Primary Visual Cortex
V2	Secondary Visual Cortex

VASO   Vascular Space Occupancy

WM   White Matter

List of Appendices

Chapter 1

1   Introduction

1.1   High-Resolution Study of the Human Brain

The human brain is an extremely complex organ that controls nearly all the body's functions. This has made it a significant research interest for decades with the overarching goal of furthering our understanding of human brain function [1]. Currently, much of this research aims at improving our understanding of brain connectivity through examining the human cerebral cortex in vivo while attempting to understand the functional organization of mesoscale circuitry [2]. If the logic behind local connectivity between functionally distinct cortical layers and columns involved in mesoscale circuitry can be revealed, it will help further our understanding of the extraordinarily convoluted connectivity [3,4] present within the human brain.

One of the main imaging modalities used to non-invasively examine human brain activity is functional magnetic resonance imaging (fMRI) [5]. fMRI provides the ability to image time-varying changes in cerebral blood oxygenation, which have been shown to be associated with changes in neural activity [5]. It is often paired with structural MRI to find the anatomical locations of the activated brain regions and it can be used macroscopically across the whole brain or locally (mesoscopically) within a specific cortical region. fMRI studies are classified as either task-based or resting-state, the former of which will be the focus of this study. Task-based fMRI is a technique that can be used to activate specific regions of the brain [6]. This is done by having the participant perform a cognitive task during the functional scan that modulates neural activity in the desired regions. The nature of the task that is used during a task-based fMRI study provides a level of control over the location of neural activity that cannot be provided with resting-state fMRI, meaning that it is beneficial when attempting to examine a particular cortical region or structure [6]. This makes task-based fMRI a useful method for investigating specific cortical functions.

Mesoscopic cortical structures such as layers and columns push the boundaries of fMRI due to their physical size and associated vascular physiology [7]. Considerable work has been done since the inception of fMRI to improve image quality, imaging resolutions, and acquisition time to help researchers examine mesoscopic cortical structures [8–10]. Increased field strengths and technical improvements in magnetic resonance (MR) hardware are some of the many advances that have recently allowed for fMRI to be used to examine functions across cortical layers (laminar fMRI) [11]. There have also been advancements in analysis techniques used over the years to enhance the processing of laminar fMRI studies [12]. However, there is still plenty of work to do before these high-resolution laminar fMRI techniques are robust.

This thesis contributes to advancing high-resolution laminar fMRI studies by further investigating techniques that aim to improve the spatial specificity of the acquisition. In the following study, fMRI combined with a technique called phase regression will be used for the first time in a laminar analysis across cortical columns in humans to determine its suitability as a technique for non-invasively examining mesoscale structures in the human brain.

1.1.1   Blood-Oxygen-Level-Dependent Contrast

The most common contrast used in fMRI is the blood-oxygen-level-dependent (BOLD) contrast, discovered by Ogawa et al. (1990) [13]. The BOLD contrast is an effect produced by paramagnetic oxygen-desaturated hemoglobin (deoxyhemoglobin) in red blood cells that is measured from water protons within blood and brain tissue when using a susceptibility-weighted pulse sequence [13]. Water is the most abundant molecule in biological tissues, with brain tissue being found to have extremely high concentrations [13]. Ogawa et al. (1990) [13] found that the concentration of water in brain tissue was too high to directly measure normal metabolic reactions, as the resonance signal was insensitive to the changes in concentration of water required for reactants. This led them to begin exploiting naturally occurring physiological events that indirectly affect the

resonance signal produced by water proton spins, such as the changes in regional cerebral blood oxygenation, which is known as the BOLD contrast [13].

When an area of the brain is stimulated, there is an increase in neuronal firing. Neural activity and the associated glial metabolism are energy intensive and require an increased supply of oxygen [14], which is provided via hemoglobin within red blood cells [15]. This link between neural activity and the corresponding changes in cerebral blood flow (CBF) and cerebral blood volume (CBV) is referred to as neurovascular coupling [16] (Figure 1.1). Neurovascular coupling allows for neural activity to be indirectly measured using changes in local blood oxygenation. Increases in CBF and CBV provide increased levels of oxygen-saturated hemoglobin (oxyhemoglobin) to areas of activation, which corresponds to a relative decrease in the local concentration of deoxyhemoglobin [13]. The reason that the changes in the level of blood oxygenation can be measured is because of the susceptibility difference of deoxyhemoglobin relative to oxyhemoglobin. While oxyhemoglobin is diamagnetic, deoxyhemoglobin is paramagnetic [17], and the paramagnetic nature of deoxyhemoglobin provides a difference in magnetic susceptibility relative to the generally diamagnetic tissue [13]. The field inhomogeneities produced by deoxyhemoglobin lead to phase dispersion of water proton spins, which reduces the BOLD signal intensity when using a susceptibility-weighted pulse sequence [13]. The presence of more oxyhemoglobin leads to less dephasing and a corresponding higher BOLD signal intensity [13]. The magnetic field variation from deoxyhemoglobin can extend beyond the boundary of the vessel to varying amounts that depend on the pulse sequence, which means there is both an intravascular and extravascular component to the BOLD signal [13]. The BOLD signal increases supra-linearly with magnetic field strength, meaning that the intravascular and extravascular components are amplified at high field strengths [13].

A Baseline | Stimulus

Artery | Vein | ● Oxyhemoglobin ● Deoxyhemoglobin

B Expected stimulus-induced changes in MR-related parameters

	Arterial Blood	Extravascular Tissue	Venous Blood	Cerebrospinal Fluid
Volume Fraction (V)	↑	↓	↑	↓
Inflow/perfusion Effect (R_1^*)	↑	↑	↑	⇔
BOLD Effect (R_2 and R_2^*)	⇔	↓	↓	↓
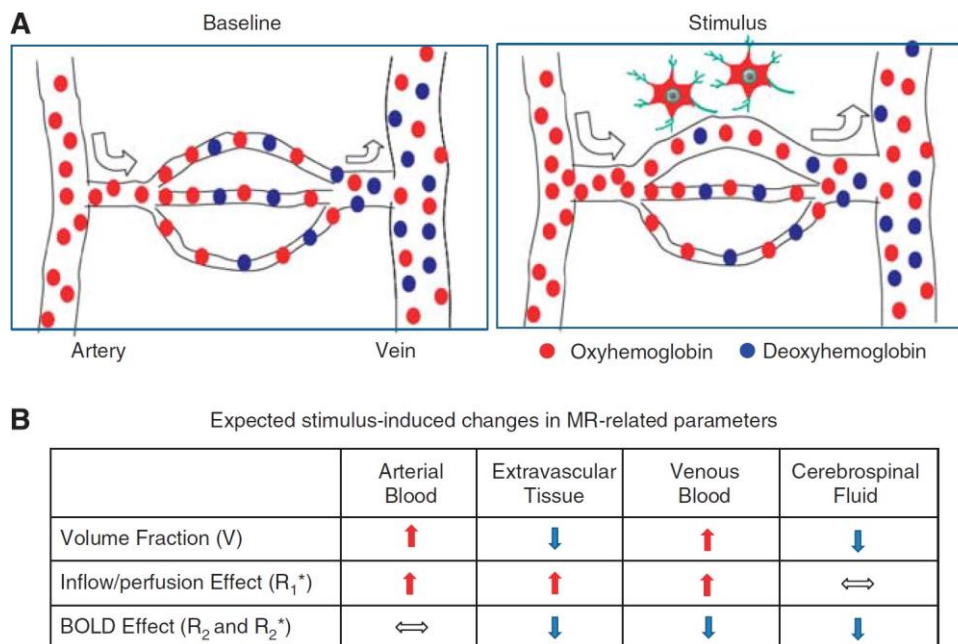
Figure 1.1. Neurovascular Coupling. A) A visualization and B) corresponding chart illustrating the changes in the volume fraction, inflow and BOLD effect in arterial blood, extravascular tissue, venous blood, and cerebrospinal fluid that correspond to neural activity. Image sourced from Kim and Ogawa (2012) [18] © 2012 SAGE Publications and reproduced with the permission of the copyright holder.

BOLD fMRI indirectly measures neural activity because it relies on neurovascular coupling to produce measurable signal changes. Neurovascular coupling is not an instantaneous process, and the temporal lag of the BOLD signal behind neural activity can be characterized by the hemodynamic response function (HRF) [18]. The HRF consists of three main components: the initial dip, the main BOLD response, and the post-stimulus undershoot (Figure 1.2). The difficult to detect initial dip in BOLD signal is a small negative response below baseline that generally lasts 1-2 seconds and is thought to be due to a local increase in deoxyhemoglobin caused by energy intensive neural activity before the corresponding increase in CBF to meet the oxygen demands [18]. The main BOLD response is the subsequent increase in oxygenated blood to the area of neural activity due to the corresponding changes in CBF and CBV [18], taking approximately 6 seconds to reach the peak in blood oxygenation and this is the portion of the BOLD signal that is typically measured. After the main BOLD response, there is a post-stimulus

undershoot where the BOLD signal again reaches a negative response before stabilizing at baseline, first showed by Kwong et al. (1992) [19]. There are two relatively common explanations mentioned when describing the post-stimulus undershoot. This first explanation is that there remains persistent increased oxygen consumption even after the duration of the stimulus, which was proposed by Frahm et al. (1996) [20] after showing large, reproducible post-stimulus undershoots. The second explanation is the balloon model proposed by Buxton et al. (1998) [21], postulating that vasodilation from the increase in CBV resulting from neural activity left a larger volume of deoxyhemoglobin than normal as CBF decreased following neural activity.
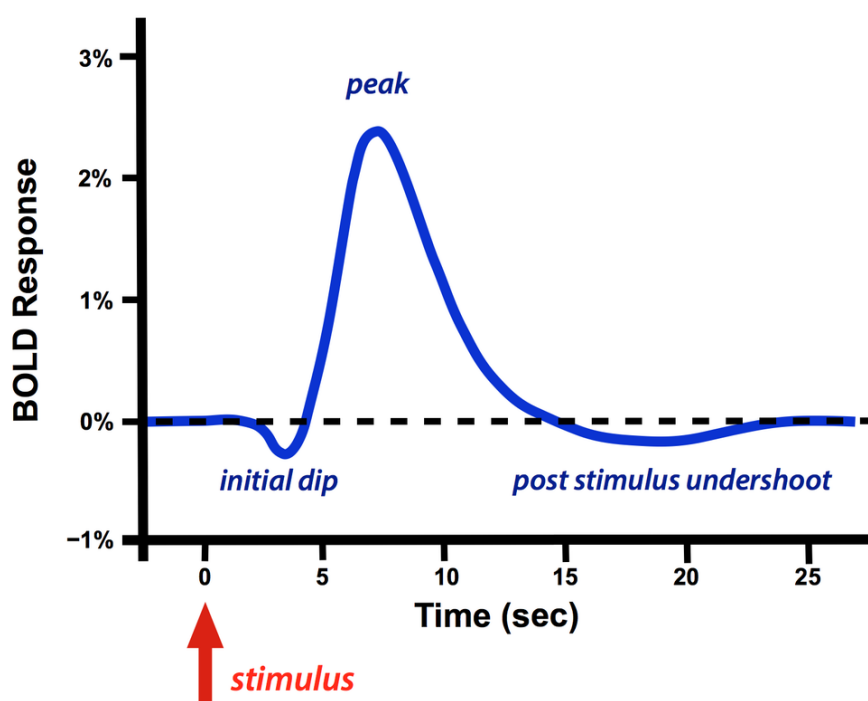
Figure 1.2. Hemodynamic Response Function. The response of the BOLD time series following a brief stimulus. The amplitudes of the response will depend on the field strength. Courtesy of Allen D. Elster, MRIquestions.com.

1.1.2 Gradient-Echo Echo-Planar Imaging

MR imaging data is collected in k-space which contains the spatial frequency distribution of the image [22]. The slice-selective (SS) gradient is used to determine the slice

thickness and location where k-space will be filled. The frequency-encoding (FE) and phase-encoding (PE) gradients are used to vary the spatial frequency and phase of the spin distribution, which manipulates the position of the signal in k-space. These two gradients are manipulated until k-space is filled. The x-axis of k-space typically corresponds to the frequency-encoding direction, while the y-axis corresponds to the phase-encoding direction. The SS gradient is then used to select a different slice where the process to fill k-space is repeated. Taking the two-dimensional inverse Fourier transform of k-space will provide the image in real space.

Gradient-echo echo-planar imaging (GE-EPI) is the most common sequence used across all fMRI studies that measures changes in the BOLD signal (Figure 1.3). In the gradient-echo (GRE) sequence [23], a radiofrequency (RF) excitation pulse is used to tip the net magnetization of spins away from the longitudinal axis towards the transverse plane at a flip angle (FA) of 90° or less, while simultaneously applying the SS gradient. The rephasing SS gradient is then applied along with the PE and FE gradients, which are used to determine the line of k-space that will be filled and to dephase the spins in the transverse plane, respectively. The echo is produced by applying the FE gradient in the opposite direction to rephase the spins in the transverse plane. The peak of the echo is when the signal is measured, and the echo time (TE) is the time from initial RF excitation pulse to the peak in the signal. This process is repeated until k-space is filled and then performed again at each slice, and the time between successive pulse sequences being applied to the same slice is called the repetition time (TR).

The FE gradient only refocuses spins that were dephased by the gradient itself and did not diffuse significantly, meaning that GRE is extremely sensitive to susceptibility in the magnetic field produced by deoxyhemoglobin [24], which cause the spins to not completely refocus in the transverse plane. This leads to a reduction in the T2* of the blood and a corresponding reduction in the intensity of a T2*-weighted image [25]. Therefore, a reduction in deoxyhemoglobin (or an increase in oxyhemoglobin) increases

the intensity of a T2*-weighted image [25]. T2* is the apparent transverse relaxation time, as opposed to T2 which is the transverse relaxation time.

Echo-planar imaging (EPI) is an MR acquisition technique invented by Mansfield (1977) [26] that is a modification of the GRE approach. It uses a rapidly reversing FE gradient with intermittent low amplitude PE gradients between reversals to fill k-space. This allows for echoes at multiple PE steps to be acquired from a single RF pulse, making it possible to rapidly obtain MR slices without needing additional RF pulses. EPI is commonly used in fMRI to allow for greatly reduced scan durations, freezing participant motion and because it is sensitive to magnetic susceptibility.
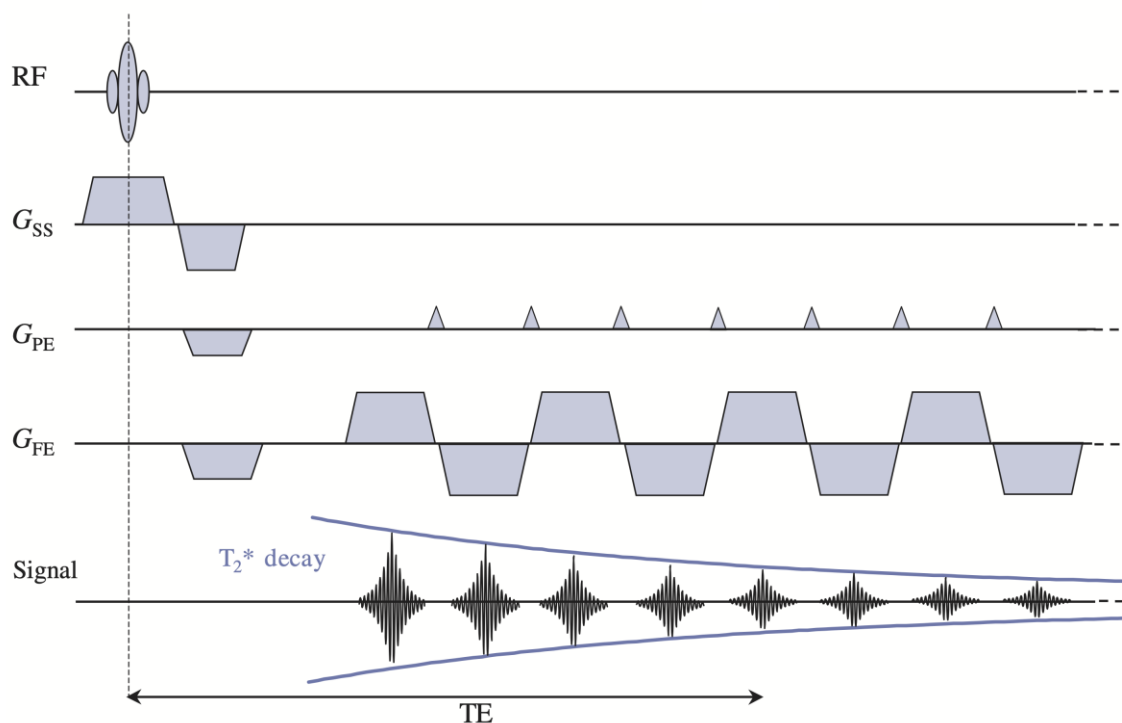
Figure 1.3. GE-EPI Pulse Sequence Diagram. A diagram illustrating the timing of the radiofrequency (RF) pulse, the slice-selective (SS), phase-encoding (PE), and frequency-encoding (FE) gradients, and the signal produced by the echoes in a GE-EPI sequence. In practice, 64-128 echoes would be used. Image sourced from McRobbie et al. (2006) [24] © 2006 Cambridge University Press and reproduced with the permission of the copyright holder.

Increasing the speed of image acquisition is nearly always desirable, but it is essential for whole-brain imaging with increased spatial and temporal resolutions [11]. Most of the commonly used acceleration techniques rely on k-space undersampling or simultaneous acquisitions. GeneRalized Autocalibrating Partially Parallel Acquisitions (GRAPPA) is a parallel imaging technique invented by Griswold et al. (2002) [8]. GRAPPA accelerates acquisition times by undersampling PE steps while fully sampling the centre of k-space and estimating the missing data from each receive coil using the weighted sensitivities of all other receive coils. Partial Fourier imaging techniques, first used by Feinberg et al. (1986) [10], use redundancies in k-space, which are conjugate symmetries diagonally across the origin of k-space. In theory, only half of k-space is needed, but realistically, this idea can be used to reconstruct MR images with approximately three quarters of k-space being sampled. Larkman et al. (2001) [9] invented Simultaneous Multi-Slice Imaging (also known as MultiBand Imaging) which is a parallel imaging technique that can excite several slices simultaneously using complex RF pulses. This allows for k-space from multiple slices to be filled simultaneously, making this an extremely useful technique for speeding up acquisitions. Combinations of acceleration techniques are usually necessary for high-resolution functional imaging [11].

The positives of GE-EPI are a high signal-to-noise ratio (SNR), as magnetic susceptibility changes increase the BOLD signal intensity [5]. GE-EPI can also be used with a low FA ($< 90°$) to use very little of the longitudinal magnetization [23]. While this will reduce the measured signal in the transverse plane, it also reduces the recovery time due to the longitudinal relaxation time (T1). This allows for a shorter repetition time (TR) as the spins can be excited more frequently, which corresponds to an increased temporal resolution [23]. This is often done to decrease the TR in GE-EPI because of the relatively high SNR per unit time of the GRE sequence. GE-EPI also has much less constraints with the specific absorption rate (SAR) than other sequences due to the reduced FA [27], allowing for an even higher temporal resolution [23]. GE-EPI paired with acceleration techniques is an extremely robust method that is simple to use, making it the main choice for most high-resolution fMRI studies.

1.2 Cortical Structure

It is important to understand the general structure of the cerebral cortex when imaging the human brain using fMRI, especially at high resolutions. The cortex is the outermost layer of neural tissue of the cerebrum. It is made up of grey matter (GM), which contains high concentrations of neuronal cell bodies and has a significant role in the higher-order functions of the human brain. The cortex exists between the cerebrospinal fluid (CSF), which surrounds the brain, and white matter (WM), which consists of myelinated axons deeper in the brain. The three features of cortical structure that will be further discussed in this work are cortical layers, cortical columns, and cortical vasculature.

Ocular dominance columns (ODCs) are cortical structures located in the primary visual cortex (V1) that have been of particular focus in high-resolution fMRI studies. Because their physiology and neuroanatomy are well understood, they are well characterized sub-millimeter cortical structures that will be helpful to test the efficacy of high-resolution fMRI acquisition techniques. Hence, the following study will focus on ODCs, and the cortical structure overview will be on the human V1.

1.2.1 Ocular Dominance Columns

One of the best studied cortical columns are ocular dominance columns (ODCs). After initially being discovered in cats using electrophysiology by Hubel and Wiesel (1962) [28], the research interest turned towards revealing ODCs in humans. They were first suggested to be present in humans by Hitchcock and Hickey (1980) [29] using Glees silver staining in post-mortem histology. ODCs were first clearly shown in humans by Horton and Hedley-Whyte (1984) [30] using cytochrome oxidase staining in post-mortem histology of patients with monocular vision loss, before Menon et al. (1997) [31] demonstrated ODCs were visible in humans using fMRI. Figure 1.4 shows ODCs in humans using a couple of the previously mentioned techniques, from Adams et al. (2007) [32] and Yacoub et al. (2007) [33]. ODCs alternate by sensitivity to input from right and left eyes in columns roughly perpendicular to the cortical surface. In humans, ODCs are

approximately 0.5-1.0 mm in width, and they are cortical structures that are restricted to V1, ending rather abruptly at the edge of V1 [32].
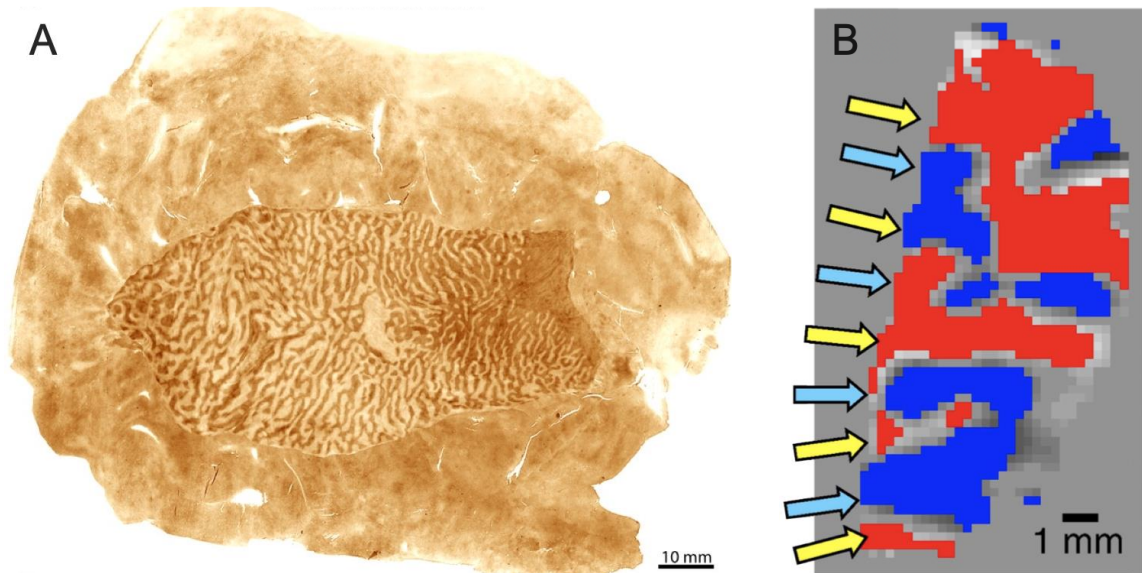
Figure 1.4. Ocular Dominance Columns. Shown using A) cytochrome oxidase staining in post-mortem histology of a patient with monocular vision loss approximately a year before death and B) the overlap of GE-EPI from three sessions. Image A adapted from Adams et al. (2007) [32] © 2007 Society for Neuroscience and reproduced with the permission of the copyright holder. Image B adapted from Yacoub et al. (2007) [33] © 2007 Elsevier Inc. and reproduced with the permission of the copyright holder.

1.2.2   Cortical Layers

The cortex can be divided into layers parallel to the cortical surface based on cell types. Although the interaction between cortical layers within V1 and with higher visual areas is extremely convoluted with feedforward and feedback processes originating at and connecting to various cortical depths, this overview will be kept relatively simple for the purpose of the following study.

In V1, there is a widely accepted six-layer structure, beginning at layer I which is the most superficial layer adjacent to the CSF and ending at layer VI, the deepest layer adjacent to the WM [2], as shown on the left side of Figure 1.6. Layer IVC (a subdivision of layer IV) receives visual information from each retina via a thalamic relay nucleus,

known as the lateral geniculate nucleus, and projects to more superficial layers [2]. Input from higher visual areas is also received mainly in superficial layers, primarily arriving from deep cortical layers [2].

Connectivity between ODCs varies as a function of cortical depth [28] (Figure 1.5). As mentioned above, layer IVC is the main input layer in V1, so this is where the signal from stimulated eyes first arrives in the cortex. This is the only cortical layer where ODCs are sensitive to segregated input from each eye [28]. In all the other cortical layers above and below layer IVC, ODCs can be sensitive to input from both eyes and the amount can vary from remaining sensitive to only one eye or equal sensitivity to both [28]. The varying mesoscale connectivity in V1 due to ODCs alternating between sensitivity to right and left eyes, along with differences in connectivity between ODCs across cortical depths makes them well suited for testing high-resolution fMRI techniques.
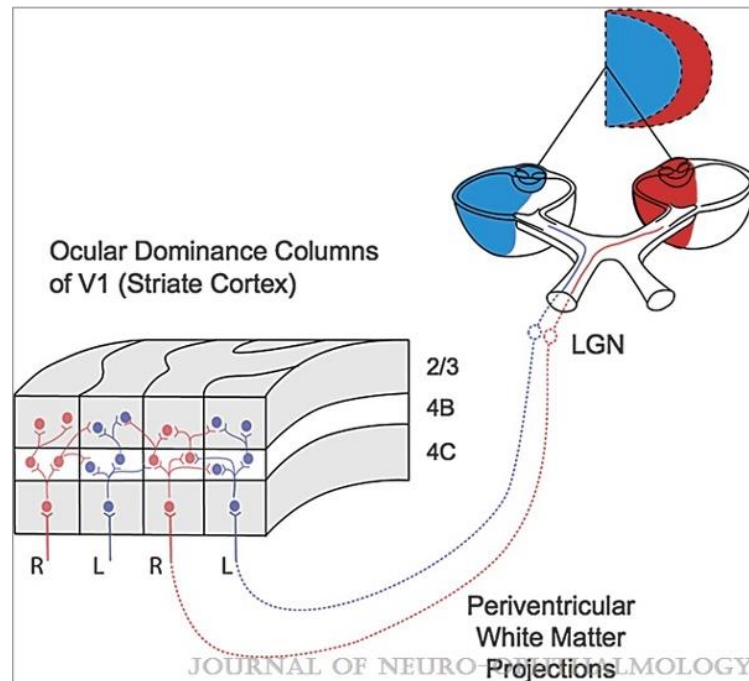
Figure 1.5. Varying Connectivity Across Cortical Layers of Ocular Dominance Columns. An example of the differences in connectivity across a few cortical layers in ocular dominance columns. Signal travels from the eyes through the lateral geniculate nucleus (LGN) and into the primary visual cortex (V1).

Monocular exclusivity is restricted to layer IVC, the main input layer in V1. Signal exchange between columns can happen in other cortical layers. Image sourced from Tychsen et al. (2010) [34] © 2010 Lippincott Williams and reproduced with the permission of the copyright holder.

1.2.3   Cortical Vasculature

Since BOLD fMRI measures a vascular response, understanding the organization of cortical vasculature and the mechanisms behind neurovascular coupling is extremely important. Blood vessels are classified into three main types: arteries, veins, and capillaries. Arteries carry oxygenated blood from the heart to the brain. Capillaries are the smallest of all the vessels, with thin walls that oxygen can most easily diffuse across to be used by the neurons within the cortex [18]. Veins carry partially deoxygenated blood from capillaries back to the heart. As arteries and veins near capillaries they decrease in size and these smaller vessels are called arterioles and venules, respectively. These three types of smaller vessels are often referred to as microvasculature. The focus of the following study primarily involves microvasculature and veins as they are what produce most of the measured BOLD signal changes at high field strengths [35].

The cortical vasculature can be divided into four layers based on vessel size, density, and orientation [36] as shown on the right side of Figure 1.6. The third vascular layer is of particular interest due to its greater vascular density, consisting of microvasculature meshes that are oriented in all directions. Vascular layers 1, 2, and 4 all contain a much lower density of microvasculature. The size and density of veins also varies across the cortex, and veins can be classified as multiple types [36]. The two largest types are pial veins, that run randomly along the cortical surface, and principal intracortical veins, that penetrate tangentially to the cortex to drain blood from the microvasculature [36]. Pial veins have a diameter of 280 µm or greater and principal intracortical veins have a diameter in the range of 80-170 µm [36]. There are also even smaller intracortical veins, reaching down to about 20 µm in diameter, that break off from principal intracortical veins and run parallel to the cortical surface at varying depths to help drain blood from the cortex [36]. The diameter of a single principal intracortical vein can vary quite drastically across cortical depths because as a principal intracortical

vein approaches the cortical surface, blood from increasing amounts of microvasculature and smaller intracortical veins will be drained to the same principal intracortical vein [36]. This causes principal intracortical veins to increase in diameter as they approach cortical surface to compensate for the increased blood volume [35]. Principal intracortical veins also vary in the depth that they penetrate the cortex, with some only reaching layers I and II [36]. This means that both the diameter and density of principal intracortical veins increase as they approach the cortical surface.
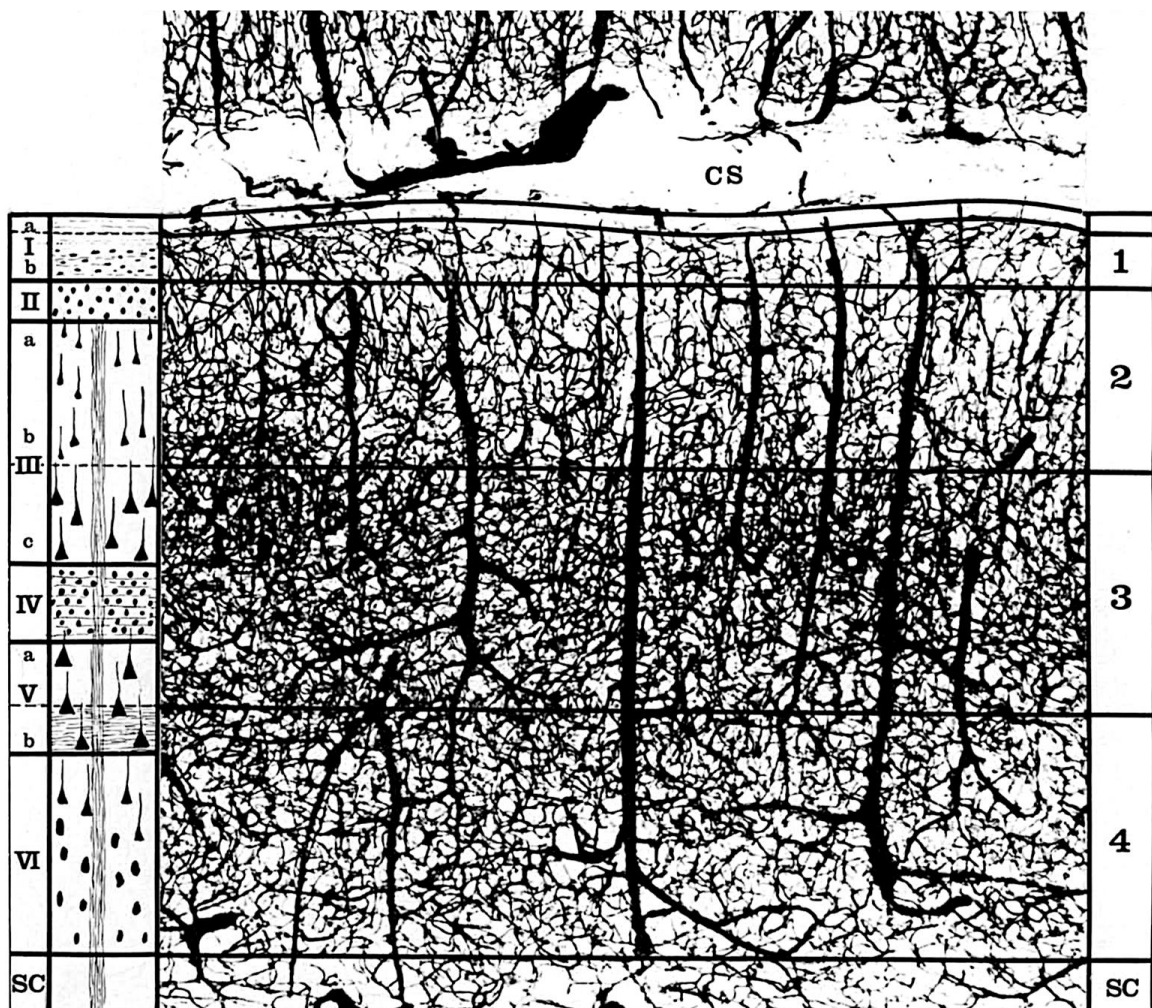
Figure 1.6. Cortical Vasculature. A cross section of the cortex outlining the six cortical layers (left) and four vasculature layers (right) from the CSF to WM (cingulate sulcus (CS) to subcortical white matter (SC), respectively). The microvasculature density is the intertangled mesh of smaller vasculature throughout the cortex, with the highest density existing in the third vasculature layer. The veins are the larger vasculature,

with a pial vein parallel to the cortical surface in the CSF, principal intracortical veins penetrating the cortex perpendicular to the cortical surface, which branch off into smaller intracortical veins running parallel to the cortical surface. Image sourced from Duvernoy et al. (1981) [36] © 1981 Elsevier Inc. and reproduced with the permission of the copyright holder.

Along with the organization of cortical vasculature, there is also a need to understand the processes behind the regulation of CBF. The three main paradigms involved with the regulation of cerebral blood flow are cerebral pressure autoregulation, flow-metabolism coupling, and neurogenic regulation [37]. Cerebral pressure autoregulation and neurogenic regulation focus more on maintaining constant CBF and are not significantly involved with neurovascular coupling [37]. Flow-metabolism coupling was first shown over a century ago and it refers to the cerebral blood flow changes that vary with cerebral metabolism [38]. This paradigm is important for the following study as we are using a task-based stimulus to induce metabolism associated with neural activity in specific regions while measuring the changes in blood oxygenation. Most of the mechanisms involved with flow-metabolism coupling are centered around metabolic causes of vasodilation, which is a significant component of neurovascular coupling [18] as shown in Figure 1.1. One of the mechanisms of flow-metabolism coupling is that synaptic activity involves potassium and hydrogen ions and the increases in these ions have been shown to stimulate vasodilation [39]. Another is that extracellular adenosine increases with neural activity, which has shown to increase microvascular vasodilation when applied topically [40]. Adenosine is also released in response to glutamate, which is one of the main neurotransmitters [41]. Nitric oxide also plays a role in flow-metabolism coupling but the exact mechanism is not completely understood [40,42]. These mechanisms primarily operate at the microvasculature level, while not operating at the artery or venous level, meaning that the microvasculature itself plays a key role in its own blood flow regulation [37]. The microvasculature is much closer to the actual site of neural activity than arteries and veins [18]. This shows that neural activity influences CBF in microvasculature, demonstrating the dependence neurovascular coupling has on flow-metabolism coupling.

1.3   fMRI Signal Spatial Specificity

Signal specificity is extremely important when performing laminar fMRI studies as non-invasive techniques indirectly measure neural activity. GE-EPI is the most common sequence used in laminar fMRI studies to date because of its increased sensitivity compared to many alternative sequences [43]. However, the blood oxygenation changes it measures are most abundant in large veins because deoxygenated blood combines downstream while draining from increased amounts of microvasculature [18,44]. The corresponding intensity changes produced by large veins dominate the BOLD signal [45,46] and due to the location, size, and density of principal intracortical veins and pial veins [36], the amount of deoxygenated blood throughout the cortex is biased towards the cortical surface [44,47,48]. This skews the measured BOLD signal towards the cortical surface (Figure 1.7), away from the microvasculature that is more tightly coupled to the neural activity [49]. Furthermore, as deoxygenated blood drains away from the microvasculature, it distances itself from areas of neural activity within the cortex [44]. This not only adds to the skewed BOLD signal towards the cortical surface, but it also displaces the BOLD signal spatially along the cortex as many venous vessels also run parallel to the cortical surface [50]. BOLD signal contamination from large veins hinders the ability to image using the BOLD contrast at high resolutions [7]. The BOLD signal changes produced exclusively by the microvasculature would be a better measure of neural activity as they are more directly related to neurovascular coupling and are in much closer proximity to the neurons, but the strength of the BOLD signal they produce is very small compared to that of larger veins because of their minimal contribution to extravascular dephasing [46]. The trade-off between SNR and spatial specificity is a major problem in laminar fMRI studies [7].
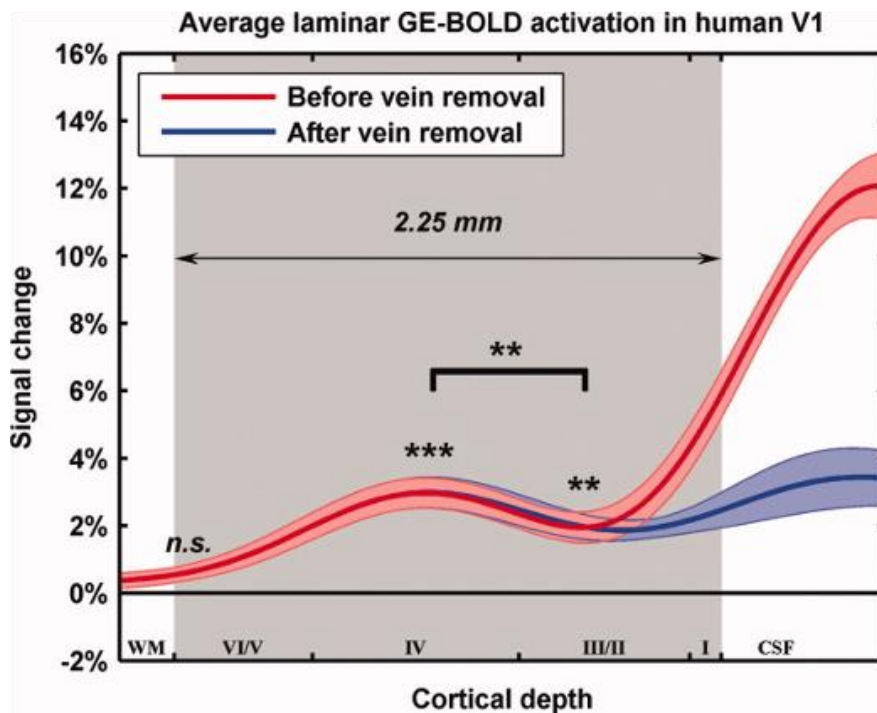
Figure 1.7. Laminar GRE BOLD Profile. An example laminar GRE BOLD profile which has a similar shape as seen in most studies (red) and one that has a shape that more accurately corresponds to neural activity (blue). Image sourced from Koopmans et al. (2010) [49] © 2010 Wiley-Liss, Inc. and reproduced with the permission of the copyright holder.

1.3.1   Alternate Imaging Contrasts

Many different acquisition techniques have been used in an attempt to combat the problem of spatial specificity in laminar fMRI studies. The first, and most easily comparable to GE-EPI, is spin-echo echo-planar imaging (SE-EPI) [51]. The SE sequence [52] is very similar to the GRE pulse sequence, with an additional 180° RF refocusing pulse after the simultaneous application of the SS, PE, and FE gradients. Instead of needing to apply a refocusing FE gradient as in GRE, the RF refocusing pulse reverses the dephasing in the transverse plane to refocus the spins. This also refocuses spins in the tissue surrounding the vasculature that were dephased due to susceptibility in the magnetic field, reducing the T2* effects produced by changes in the concentration of deoxyhemoglobin from the signal, producing a more T2-weighted image. The measured signal in T2-weighted images is much more specific to microvasculature due to the

reduction in T2* effects that are most prominent around large veins [46]. Although SE-EPI has higher spatial specificity compared to GE-EPI, it has a considerably reduced SNR because of the inversion pulse used to reduce the T2* effects, which reduces the amount of spins that are producing the measured signal [7]. The additional refocusing pulse also lengthens the TE, along with being more SAR-intensive [27].

Another alternate sequence that has gained interest in laminar fMRI studies is vascular space occupancy (VASO) [53]. VASO is based on changes in CBV, which primarily happens in microvasculature, as large vessels are unimportant for the local regulation of blood flow during neural activity [53]. This method relies on the T1 difference between blood and the surrounding tissue. It uses a 180° RF nonselective inversion pulse to invert the magnetization in the longitudinal plane. The blood signal is nulled by waiting to perform the 90° RF excitation pulse until the longitudinal magnetization of blood crosses zero, leaving only signal produced by the surrounding tissue and extravascular BOLD changes [53]. BOLD data is also acquired so it can be used to remove T2* contamination from the surrounding tissue [53]. Neural activity causes an increase in microvascular CBV, which reduces the measured signal from the surrounding tissue [53]. Due to the inverse relationship with CBV (i.e., the extravascular signal decreases with increased CBV), a negative signal change is expected in VASO. While VASO is specific to microvasculature, it has considerably lower SNR because only a limited tissue signal remains at the time of blood nulling. The amount of signal remaining decreases even further with higher magnetic field strengths because it reduces the T1 difference between blood and tissue [54]. VASO also has a much lower temporal resolution than GE-EPI because of the need to wait for the longitudinal magnetization to completely revert before a subsequent RF inversion pulse [53].

These are only brief overviews of two of the most common alternatives to GE-EPI. Even with other sequences that have superior spatial specificity, GE-EPI is still the most common sequence due to its higher SNR, which many deem the single most limiting factor in laminar fMRI.

1.3.2   Venous Bias Correction Techniques

Instead of sacrificing SNR for one of the previously mentioned more spatially specific sequences, there have been many techniques paired with GRE BOLD to help increase its spatial specificity by reducing the venous bias while maintaining a higher SNR. These techniques vary from additional imaging to postprocessing steps and everything in between, some of which will be mentioned here.

One technique used recently in an ODC study by Hollander et al. (2021) [55] was deconvolution based on the cortical vascular model described in Markuerkiaga et al. (2016) [47]. The model was formulated from the distribution of microvasculature and density of intracortical veins throughout the cortex. It only included intracortical veins and microvasculature (no pial veins) to simulate BOLD signal across cortical depths for GRE BOLD and SE-BOLD. This cortical vascular model was used to determine the weighting factors for the spatial deconvolution [56]. While this method does assist in the removal of the venous bias, it is still based on a generalization of cortical vasculature.

Another technique proposed for increasing the spatial specificity of GRE BOLD was by imaging at a higher spatial resolution and then excluding the upper cortical layers from the analysis [57]. In this technique, only the deep and middle cortical layers are kept in the analysis. This attempts to avoid pial veins along the cortical surface and partial volume effects with CSF, both of which reduce the spatial specificity of the BOLD signal. By removing the superficial layers from the analysis, it effectively provides a BOLD signal that is more specific to layer IV. One downside to this technique is that it also removes any true signal produced by superficial neuronal activity when removing the venous bias from the superficial layers.

There is also a technique involved with examining the initial dip of the BOLD response [58]. It was shown that the magnitude of the initial dip is dependent on cortical depth, which can be used to improve the localization of functional activation. However, the signal amplitude in the initial dip is extremely small, especially at deeper cortical

layers. While this provides an understanding of the location of the responses at varying cortical depths, it doesn't necessarily assist in removing venous bias from the analysis.

These are only a few of many venous bias correction techniques that have been proposed. Due to the vast differences between techniques, they all have significantly varying pros and cons. As of now, there is still no consensus on the ideal venous bias correction technique. This only adds to the difficult choice between a more spatially specific imaging sequence or one of the many venous bias correction techniques commonly paired with GRE BOLD, and a considerable amount of research is still dedicated to finding the ideal method for performing laminar fMRI studies.

1.3.3   Phase Regression

One technique that uses phase data to remove the venous bias from the corresponding GRE BOLD magnitude data, now referred to as phase regression, was first proposed by Menon (2002) [59]. It is important to note that fMRI is a complex valued imaging modality. This is commonly represented as magnitude and phase data, with phase data typically being discarded. However, it has been shown that phase data contains valuable information that can be used to correct for field distortions [60], physiological noise [61], and venous bias [59]. In the following study, the main use of phase data will be for removing the venous bias from magnitude data.

Menon et al. (2002) [59] showed that varying sizes and orientations of vasculature will produce different effects in both the magnitude and phase data. Large veins contribute to significant portions of the magnitude data, while also producing measurable changes in phase data [59]. Microvasculature contributes to a smaller amount of the magnitude data and produces minimal changes in phase data [59]. These differences in phase changes produced by large veins and microvasculature allow the large vein contribution in magnitude data to be estimated [59]. The estimate of the large vein contribution in magnitude data can then be subtracted from the native magnitude to leave the portion of the data that is more specific to microvasculature (phase regressed data).

It has been shown that it is unlikely one can obtain useful phase information from vasculature under 150 µm in diameter [62], meaning that phase regression will only be effective on pial surface veins and large principal intracortical veins. At low resolutions, phase changes related to the BOLD signal are predominantly from intravascular changes [45,59]. At high resolutions, phase regression has been shown to be effective at suppressing both the intravascular and extravascular BOLD components, increasing the reduction of venous bias [63]. Pairing phase regression with GRE BOLD will provide it with increased spatial specificity while maintaining a relatively high SNR [63]. This potentially makes it better suited for laminar fMRI studies

1.4   Thesis Objectives

Laminar fMRI is an area of research that has attracted increasing interest over recent years due to advancements in fMRI acquisition and analysis techniques [64,65] that have increased our potential for understanding the functional organization of mesoscale circuitry in the human brain [66]. This thesis looks to further laminar fMRI techniques, with the primary focus on the use of phase data to remove the venous bias from the GRE BOLD signal. Phase regression is expected to provide GRE BOLD with improved spatial specificity to allow for the investigation of mesoscopic cortical structures. The main objective of this thesis was to investigate the effectiveness of GRE BOLD with phase regression for high-resolution laminar and columnar studies in the human V1.

Chapter 2 investigates using GRE BOLD with phase regression as a technique for high-resolution laminar and columnar studies by imaging ODCs across cortical depths in human V1 at 7 T. Phase regression's improvements in spatial specificity were determined through examining ODCs using a task-based experiment, with and without phase regression. We hypothesized that GRE BOLD with phase regression will provide more defined ODCs by removing BOLD signal distant to the neural activity, that the laminar BOLD signal profile will peak in the middle of the cortex after removing the venous bias, and that the difference between right and left eye specificity in ODCs will be greatest in layer IVC where ODCs are exclusively receive input from a single eye.

The final chapter of this thesis discusses and summarizes the findings of this study. The study limitations will be thoroughly discussed before providing recommendations on future directions related to high-resolution BOLD fMRI with phase regression.

1.5   References

[1] M.E. Raichle, A brief history of human brain mapping, Trends Neurosci. 32 (2009) 118–126. https://doi.org/10.1016/j.tins.2008.11.001.

[2] R.J. Douglas, K.A.C. Martin, Neuronal Circuits of the Neocortex, Neuroscience. 27 (2004) 419–451. https://doi.org/10.1146/annurev.neuro.27.070203.144152.

[3] J.S. Lund, Anatomical Organization of Macaque Monkey Striate Visual Cortex, Annu Rev Neurosci. 11 (1988) 253–288. https://doi.org/10.1146/annurev.ne.11.030188.001345.

[4] E.M. Callaway, Local Circuits in Primary Visual Cortex of the Macaque Monkey, Annu Rev Neurosci. 21 (1998) 47–74. https://doi.org/10.1146/annurev.neuro.21.1.47.

[5] S. Ogawa, T.M. Lee, A.R. Kay, D.W. Tank, Brain magnetic resonance imaging with contrast dependent on blood oxygenation., Proc National Acad Sci. 87 (1990) 9868–9872. https://doi.org/10.1073/pnas.87.24.9868.

[6] N.K. Logothetis, What we can do and what we cannot do with fMRI, Nature. 453 (2008) 869–878. https://doi.org/10.1038/nature06976.

[7] R.S. Menon, The great brain versus vein debate, Neuroimage. 62 (2012) 970–974. https://doi.org/10.1016/j.neuroimage.2011.09.005.

[8] M.A. Griswold, P.M. Jakob, R.M. Heidemann, M. Nittka, V. Jellus, J. Wang, B. Kiefer, A. Haase, Generalized autocalibrating partially parallel acquisitions (GRAPPA), Magn. Reson. Med. 47 (2002) 1202–1210. https://doi.org/10.1002/mrm.10171.

[9] D.J. Larkman, J.V. Hajnal, A.H. Herlihy, G.A. Coutts, I.R. Young, G. Ehnholm, Use of multicoil arrays for separation of signal from multiple slices simultaneously excited, J. Magn. Reson. Imaging. 13 (2001) 313–317. https://doi.org/10.1002/1522-2586(200102)13:2<313::aid-jmri1045>3.0.co;2-w.

[10] D.A. Feinberg, J.D. Hale, J.C. Watts, L. Kaufman, A. Mark, Halving MR imaging time by conjugation: demonstration at 3.5 kG., Radiology. 161 (1986) 527–531. https://doi.org/10.1148/radiology.161.2.3763926.

[11] K. Uğurbil, Imaging at ultrahigh magnetic fields: History, challenges, and solutions, Neuroimage. 168 (2018) 7–32. https://doi.org/10.1016/j.neuroimage.2017.07.007.

[12] L. (Renzo) Huber, B.A. Poser, P.A. Bandettini, K. Arora, K. Wagstyl, S. Cho, J. Goense, N. Nothnagel, A.T. Morgan, J. van den Hurk, A.K. Müller, R.C. Reynolds, D.R. Glen, R. Goebel, O.F. Gulban, LayNii: A software suite for layer-fMRI, Neuroimage. 237 (2021) 118091. https://doi.org/10.1016/j.neuroimage.2021.118091.

[13] S. Ogawa, T. Lee, A.S. Nayak, P. Glynn, Oxygenation-sensitive contrast in magnetic resonance image of rodent brain at high magnetic fields, Magnet Reson Med. 14 (1990) 68–78. https://doi.org/10.1002/mrm.1910140108.

[14] G.A. Dienel, L. Hertz, Glucose and lactate metabolism during brain activation, J. Neurosci. Res. 66 (2001) 824–838. https://doi.org/10.1002/jnr.10079.

[15] F. Schmid, M.J.P. Barrett, D. Obrist, B. Weber, P. Jenny, Red blood cells stabilize flow in brain microvascular networks, Plos Comput Biol. 15 (2019) e1007231. https://doi.org/10.1371/journal.pcbi.1007231.

[16] A.A. Phillips, F.H. Chan, M.M.Z. Zheng, A.V. Krassioukov, P.N. Ainslie, Neurovascular coupling in humans: Physiology, methodological advances and clinical implications, J Cereb Blood Flow Metabolism. 36 (2015) 647–664. https://doi.org/10.1177/0271678x15617954.

[17] L. Pauling, C.D. Coryell, The Magnetic Properties and Structure of Hemoglobin, Oxyhemoglobin and Carbonmonoxyhemoglobin, Proc National Acad Sci. 22 (1936) 210–216. https://doi.org/10.1073/pnas.22.4.210.

[18] S.-G. Kim, S. Ogawa, Biophysical and Physiological Origins of Blood Oxygenation Level-Dependent fMRI Signals, J Cereb Blood Flow Metabolism. 32 (2012) 1188–1206. https://doi.org/10.1038/jcbfm.2012.23.

[19] K.K. Kwong, J.W. Belliveau, D.A. Chesler, I.E. Goldberg, R.M. Weisskoff, B.P. Poncelet, D.N. Kennedy, B.E. Hoppel, M.S. Cohen, R. Turner, Dynamic magnetic resonance imaging of human brain activity during primary sensory stimulation., Proc National Acad Sci. 89 (1992) 5675–5679. https://doi.org/10.1073/pnas.89.12.5675.

[20] J. Frahm, G. Krüger, K. Merboldt, A. Kleinschmidt, Dynamic uncoupling and recoupling of perfusion and oxidative metabolism during focal brain activation in man, Magn. Reson. Med. 35 (1996) 143–148. https://doi.org/10.1002/mrm.1910350202.

[21] R.B. Buxton, E.C. Wong, L.R. Frank, Dynamics of blood flow and oxygenation changes during brain activation: The balloon model, Magn. Reson. Med. 39 (1998) 855–864. https://doi.org/10.1002/mrm.1910390602.

[22] T.R. Brown, B.M. Kincaid, K. Ugurbil, NMR chemical shift imaging in three dimensions., Proc National Acad Sci. 79 (1982) 3523–3526. https://doi.org/10.1073/pnas.79.11.3523.

[23] A. Haase, J. Frahm, D. Matthaei, W. Hanicke, K.-D. Merboldt, FLASH imaging. Rapid NMR imaging using low flip-angle pulses, J Magnetic Reson 1969. 67 (1986) 258–266. https://doi.org/10.1016/0022-2364(86)90433-6.

[24] D.W. McRobbie, E.A. Moore, M.J. Graves, M.R. Prince, MRI: From Picture to Proton, 2nd ed., Cambridge University Press, Cambridge, New York, Melbourne, Madrid, Cape Town, Singapore, São Paulo, 2006. https://doi.org/10.1017/cbo9780511545405.

[25] K.R. Thulborn, J.C. Waterton, P.M. Matthews, G.K. Radda, Oxygenation dependence of the transverse relaxation time of water protons in whole blood at high field, Biochimica Et Biophysica Acta Bba - Gen Subj. 714 (1982) 265–270. https://doi.org/10.1016/0304-4165(82)90333-6.

[26] P. Mansfield, Multi-planar image formation using NMR spin echoes, J Phys C Solid State Phys. 10 (1977) L55. https://doi.org/10.1088/0022-3719/10/3/004.

[27] J.E.H. Prost, F.W. Wehrli, B. Drayer, J. Froelich, D. Hearshen, D. Plewes, SAR reduced pulse sequences, Magn Reson Imaging. 6 (1988) 125–130. https://doi.org/10.1016/0730-725x(88)90441-9.

[28] D.H. Hubel, T.N. Wiesel, Receptive fields, binocular interaction and functional architecture in the cat's visual cortex, J Physiology. 160 (1962) 106–154. https://doi.org/10.1113/jphysiol.1962.sp006837.

[29] P.F. Hitchcock, T.L. Hickey, Ocular dominance columns: evidence for their presence in humans, Brain Res. 182 (1980) 176–179. https://doi.org/10.1016/0006-8993(80)90841-0.

[30] J.C. Horton, E.T. Hedley-Whyte, Mapping of cytochrome oxidase patches and ocular dominance columns in human visual cortex, Philosophical Transactions Royal Soc Lond B Biological Sci. 304 (1984) 255–272. https://doi.org/10.1098/rstb.1984.0022.

[31] R.S. Menon, S. Ogawa, J.P. Strupp, K. Uğurbil, Ocular Dominance in Human V1 Demonstrated by Functional Magnetic Resonance Imaging, J Neurophysiol. 77 (1997) 2780–2787. https://doi.org/10.1152/jn.1997.77.5.2780.

[32] D.L. Adams, L.C. Sincich, J.C. Horton, Complete Pattern of Ocular Dominance Columns in Human Primary Visual Cortex, J Neurosci. 27 (2007) 10391–10403. https://doi.org/10.1523/jneurosci.2923-07.2007.

[33] E. Yacoub, A. Shmuel, N. Logothetis, K. Uğurbil, Robust detection of ocular dominance columns in humans using Hahn Spin Echo BOLD functional MRI at 7 Tesla, Neuroimage. 37 (2007) 1161–1177. https://doi.org/10.1016/j.neuroimage.2007.05.020.

[34] L. Tychsen, M. Richards, A. Wong, P. Foeller, D. Bradley, A. Burkhalter, The Neural Mechanism for Latent (Fusion Maldevelopment) Nystagmus, J Neuro-Ophthalmol. 30 (2010) 276–283. https://doi.org/10.1097/wno.0b013e3181dfa9ca.

[35] K. Uludağ, B. Müller-Bierl, K. Uğurbil, An integrative model for neuronal activity-induced signal changes for gradient and spin echo functional imaging, Neuroimage. 48 (2009) 150–165. https://doi.org/10.1016/j.neuroimage.2009.05.051.

[36] H.M. Duvernoy, S. Delon, J.L. Vannson, Cortical blood vessels of the human brain, Brain Res Bull. 7 (1981) 519–579. https://doi.org/10.1016/0361-9230(81)90007-1.

[37] E.C. Peterson, Z. Wang, G. Britz, Regulation of Cerebral Blood Flow, Int J Vasc Medicine. 2011 (2011) 823525. https://doi.org/10.1155/2011/823525.

[38] C.S. Roy, C.S. Sherrington, On the Regulation of the Blood-supply of the Brain, J Physiology. 11 (1890) 85–158. https://doi.org/10.1113/jphysiol.1890.sp000321.

[39] O.B. Paulson, E.A. Newman, Does the Release of Potassium from Astrocyte Endfeet Regulate Cerebral Blood Flow?, Science. 237 (1987) 896–898. https://doi.org/10.1126/science.3616619.

[40] D.A. Pelligrino, R.L. Gay, V.L. Baughman, Q. Wang, NO synthase inhibition modulates NMDA-induced changes in cerebral blood flow and EEG activity, Am J Physiol-Heart C. 271 (1996) H990–H995. https://doi.org/10.1152/ajpheart.1996.271.3.h990.

[41] K. Hoehn, T.D. White, Role of Excitatory Amino Acid Receptors in K+-and Glutamate-Evoked Release of Endogenous Adenosine from Rat Cortical Slices, J Neurochem. 54 (1990) 256–265. https://doi.org/10.1111/j.1471-4159.1990.tb13309.x.

[42] F.M. Faraci, K.R. Breese, Nitric oxide mediates vasodilatation in response to activation of N-methyl-D-aspartate receptors in brain., Circ Res. 72 (1993) 476–480. https://doi.org/10.1161/01.res.72.2.476.

[43] M. Moerel, F.D. Martino, V.G. Kemper, S. Schmitter, A.T. Vu, K. Uğurbil, E. Formisano, E. Yacoub, Sensitivity and specificity considerations for fMRI encoding, decoding, and mapping of auditory cortex at ultra-high field, Neuroimage. 164 (2018) 18–31. https://doi.org/10.1016/j.neuroimage.2017.03.063.

[44] R. Turner, How Much Cortex Can a Vein Drain? Downstream Dilution of Activation-Related Cerebral Blood Oxygenation Changes, Neuroimage. 16 (2002) 1062–1067. https://doi.org/10.1006/nimg.2002.1082.

[45] S. Ogawa, R.S. Menon, D.W. Tank, S.G. Kim, H. Merkle, J.M. Ellermann, K. Ugurbil, Functional brain mapping by blood oxygenation level-dependent contrast magnetic resonance imaging. A comparison of signal characteristics with a biophysical model, Biophys J. 64 (1993) 803–812. https://doi.org/10.1016/s0006-3495(93)81441-3.

[46] F.G.C. Hoogenraad, P.J.W. Pouwels, M.B.M. Hofman, J.R. Reichenbach, M. Sprenger, E.M. Haacke, Quantitative differentiation between BOLD models in fMRI, Magn. Reson. Med. 45 (2001) 233–246. https://doi.org/10.1002/1522-2594(200102)45:2<233::aid-mrm1032>3.0.co;2-w.

[47] I. Markuerkiaga, M. Barth, D.G. Norris, A cortical vascular model for examining the specificity of the laminar BOLD signal, Neuroimage. 132 (2016) 491–498. https://doi.org/10.1016/j.neuroimage.2016.02.073.

[48] K. Uludağ, P. Blinder, Linking brain vascular physiology to hemodynamic response in ultra-high field MRI, Neuroimage. 168 (2018) 279–295. https://doi.org/10.1016/j.neuroimage.2017.02.063.

[49] P.J. Koopmans, M. Barth, D.G. Norris, Layer-specific BOLD activation in human V1, Hum Brain Mapp. 31 (2010) 1297–1304. https://doi.org/10.1002/hbm.20936.

[50] C.A. Olman, S. Inati, D.J. Heeger, The effect of large veins on spatial localization with GE BOLD at 3 T: Displacement, not blurring, Neuroimage. 34 (2007) 1126–1135. https://doi.org/10.1016/j.neuroimage.2006.08.045.

[51] J.B.M. Goense, N.K. Logothetis, Laminar specificity in monkey V1 using high-resolution SE-fMRI, Magn Reson Imaging. 24 (2006) 381–392. https://doi.org/10.1016/j.mri.2005.12.032.

[52] E.L. Hahn, Spin Echoes, Phys Rev. 80 (1950) 580–594. https://doi.org/10.1103/physrev.80.580.

[53] H. Lu, X. Golay, J.J. Pekar, P.C.M. van Zijl, Functional magnetic resonance imaging based on changes in vascular space occupancy, Magnet Reson Med. 50 (2003) 263–274. https://doi.org/10.1002/mrm.10519.

[54] T. Jin, S.-G. Kim, Improved cortical-layer specificity of vascular space occupancy fMRI with slab inversion relative to spin-echo BOLD at 9.4 T, Neuroimage. 40 (2008) 59–67. https://doi.org/10.1016/j.neuroimage.2007.11.045.

[55] G. de Hollander, W. van der Zwaag, C. Qian, P. Zhang, T. Knapen, Ultra-high field fMRI reveals origins of feedforward and feedback activity within laminae of human ocular dominance columns, Neuroimage. 228 (2021) 117683. https://doi.org/10.1016/j.neuroimage.2020.117683.

[56] I. Marquardt, M. Schneider, O.F. Gulban, D. Ivanov, K. Uludağ, Cortical depth profiles of luminance contrast responses in human V1 and V2 using 7 T fMRI, Hum Brain Mapp. 39 (2018) 2812–2827. https://doi.org/10.1002/hbm.24042.

[57] J.R. Polimeni, B. Fischl, D.N. Greve, L.L. Wald, Laminar analysis of 7T BOLD using an imposed spatial activation pattern in human V1, Neuroimage. 52 (2010) 1334–1346. https://doi.org/10.1016/j.neuroimage.2010.05.005.

[58] J.C.W. Siero, J. Hendrikse, H. Hoogduin, N. Petridou, P. Luijten, M.J. Donahue, Cortical depth dependence of the BOLD initial dip and poststimulus undershoot in human visual cortex at 7 Tesla, Magnet Reson Med. 73 (2015) 2283–2295. https://doi.org/10.1002/mrm.25349.

[59] R.S. Menon, Postacquisition suppression of large-vessel BOLD signals in high-resolution fMRI, Magnet Reson Med. 47 (2002) 1–9. https://doi.org/10.1002/mrm.10041.

[60] B. Dymerska, B.A. Poser, M. Barth, S. Trattnig, S.D. Robinson, A method for the dynamic correction of B0-related distortions in single-echo EPI at 7T, Neuroimage. 168 (2018) 321–331. https://doi.org/10.1016/j.neuroimage.2016.07.009.

[61] A.T. Curtis, R.S. Menon, Highcor: A novel data-driven regressor identification method for BOLD fMRI, Neuroimage. 98 (2014) 184–194. https://doi.org/10.1016/j.neuroimage.2014.05.013.

[62] M. Klassen, R.S. Menon, BOLD Phase and Mag Dependance on Vessel Geometry, Proceedings of the 13th International Society for Magnetic Resonance in Medicine Annual Meeting. (2005).

[63] O.W. Stanley, A.B. Kuurstra, L.M. Klassen, R.S. Menon, J.S. Gati, Effects of phase regression on high-resolution functional MRI of the primary visual cortex, Neuroimage. 227 (2021) 117631. https://doi.org/10.1016/j.neuroimage.2020.117631.

[64] L. Huber, E.S. Finn, Y. Chai, R. Goebel, R. Stirnberg, T. Stöcker, S. Marrett, K. Uludag, S.G. Kim, S. Han, P.A. Bandettini, B.A. Poser, Layer-dependent functional connectivity methods, Prog Neurobiol. (2020) 101835. https://doi.org/10.1016/j.pneurobio.2020.101835.

[65] J.R. Polimeni, V. Renvall, N. Zaretskaya, B. Fischl, Analysis strategies for high-resolution UHF-fMRI data, Neuroimage. 168 (2018) 296–320. https://doi.org/10.1016/j.neuroimage.2017.04.053.

[66] S.J.D. Lawrence, E. Formisano, L. Muckli, F.P. de Lange, Laminar fMRI: Applications for cognitive neuroscience, Neuroimage. 197 (2019) 785–791. https://doi.org/10.1016/j.neuroimage.2017.07.004.

Chapter 2

2 Depth-Dependent Analysis of Human Ocular Dominance Columns using BOLD fMRI with Phase Regression at 7 T

This study investigated the signal spatial specificity of the gradient-echo blood-oxygen-level-dependent (GRE BOLD) contrast with and without phase regression across layers of the human primary visual cortex (V1) in ocular dominance columns (ODCs) at 7 T. Phase regression is a post-processing technique that uses phase data to suppress large vein signal, thus improving the GRE signal spatial specificity. A task-based fMRI study was performed where the visual stimulus was presented to the participants monocularly and binocularly. The depth-dependent and column-specific BOLD profiles with and without the phase regression were obtained in V1 to examine the spatial specificity of the phase regressed BOLD signal. Our results showed that the phase regressed laminar BOLD profile peaked towards the middle cortical depth, while that of GRE BOLD was biased towards the cortical surface. However, phase regression failed to improve the contrast between right and left eye ODCs, suggesting that we could not obtain useful phase information from venous vessel sizes running parallel to the cortical surface at various depths.

2.1   Introduction

Laminar fMRI studies typically use high field strengths to provide an improved signal-to-noise ratio (SNR) that allows for functional imaging with sub-millimeter voxels [1]. High-resolution imaging provides researchers with the ability to study cortical layers and columns non-invasively in both animals and humans [2–4]. Input and output in primary sensory regions are located in different cortical layers and they are associated with feedforward and feedback activity [5]. Studying local functional connectivity between cortical layers could improve our understanding of feedforward and feedback activity within the visual areas of the human brain [6].

One of the best studied cortical columnar structures in the human brain are ocular dominance columns (ODCs) [7]. They are located within the primary visual cortex (V1) and are predominantly sensitive to input from a specific eye [7]. ODCs alternate in columns roughly perpendicular to the cortical surface, approximately 0.5-1.0 mm in width, spanning across the entire V1 [8]. While ODCs exist across all cortical depths, monocular input is specific to layer IVC [7]. Above and below layer IVC, ODCs have varying amounts of signal exchange between columns [7]. While ODCs have been shown non-invasively in humans using fMRI, they are commonly imaged with anisotropic voxels and without specifying differences in cortical depths [9–11]. Only recently have they been shown with sub-millimeter isotropic voxels that allows for depth-dependent analysis across the layers of the columns [4].

The most common MR sequence used in laminar fMRI studies to date is gradient-echo echo-planar imaging (GE-EPI). GE-EPI measures the blood-oxygen-level-dependent (BOLD) signal change, which is an fMRI contrast that relies on changes in the concentration of deoxyhemoglobin within the blood [12,13]. GE-EPI comes with one major downside of not being specific to microvasculature (i.e., capillaries and venules) in the cortex [14,15]. Large veins dominate the BOLD signal changes and skew the signal towards the cortical surface due to their location, size, and density [16–18]. This makes it difficult to pinpoint the laminar origin of the BOLD signal even when imaging at higher resolutions [19,20]. To conduct a laminar fMRI study with greater signal specificity, the BOLD signal originating from large veins needs to be reduced [14].

There have been multiple acquisition and post-processing techniques used to suppress the BOLD signal change originating from large veins. The two most common alternate MR acquisition techniques used in laminar fMRI are spin-echo EPI (SE-EPI) [21] and vascular space occupancy (VASO) [22], both of which have shown better signal spatial specificity compared to BOLD. Post-processing methods have also been proposed to reduce the venous signal contribution. A deconvolution approach based on a cortical vascular model [16], eliminating the voxels located in superficial cortical layers from the

analysis [23] or using the initial dip of the BOLD response [24], are among the post-processing methods that have been used with some success.

Phase regression is a data-driven approach to suppress the BOLD signal from large veins and relies on the fact that magnitude data contains signal contribution from large veins and microvasculature, while phase data mainly reflects the venous signal change [25]. The correspondence between magnitude and phase data produced from large veins allows the phase data to be used to estimate the BOLD signal contribution from large veins and suppress their effect. Phase regression was originally used at lower resolutions [25–32] although it has recently been shown to also be effective at higher resolutions [33]. Stanley et al. (2020) [33] compared the sensitivity and specificity of phase regressed GRE BOLD signal with the SE and native GRE BOLD signal and showed that phase regression provides a comparable specificity to SE, yet higher signal sensitivity. Thus, phase regression promises a more spatially specific GRE BOLD signal both parallel and perpendicular to the cortical surface. This could make it well suited for laminar and columnar studies.

In the current study, we investigated the GRE BOLD signal spatial specificity and sensitivity for imaging the ocular dominance columns with and without phase regression in order to determine if differences in interactions between columns at specific cortical depths can be revealed. We expected that GRE BOLD with phase regression will produce better defined columns by removing downstream BOLD signal distant to the site of neural activity. It is hypothesized that the laminar BOLD signal profile from GRE with phase regression will peak in the middle of the cortex, corresponding to the density of the microvasculature across the cortex. It is also hypothesized that the difference between right and left eye sensitivity in ODCs will be greatest in the middle of the cortex where ODCs exclusively receive signal from a specific eye, when using GRE BOLD with phase regression.

2.2   Methods

2.2.1   Data Acquisition

2.2.1.1   Participant Characteristics

Data was acquired from five participants (3 females and 2 males; age range 22-35 years). To ensure each participant had appropriate stereo vision, they performed the Randot Stereotest (Stereo Optical, Inc., Chicago, IL) prior to imaging and all participants fell within the normal or borderline normal range. Informed consent was collected from all participants and approved by the Human Subjects Research Ethics Board at the University of Western Ontario.

2.2.1.2   Imaging Protocol

Imaging was performed with a 7 T MRI scanner (Siemens MAGNETOM 7 T MRI Plus, Erlangen, Germany) optimized for the human brain imaging, equipped with an AC84 II head gradient coil. Functional data was collected using an 8-channel Tx/32-channel Rx radiofrequency (RF) coil optimized for occipital-parietal imaging [34]. For the functional imaging, the data collected was axial-oblique GE-EPI centered around the calcarine sulcus with the following imaging parameters: isotropic resolution = 0.8 mm^3; TE = 23.8 ms; TR = 1 s; FA = 50°; GRAPPA acceleration factor = 3; partial Fourier 6/8; MultiBand = 2. Each participant performed two functional imaging sessions with the same GE-EPI sequence: one for imaging the ODCs and one for performing retinotopy. The retinotopy consisted of meridian mapping for localizing V1. The ODC session consisted of 5 runs of 600 volumes each and the retinotopy session consisted of 4 runs of 324 volumes each. The structural data was collected using an 8-channel Tx/32-channel Rx whole head RF coil and used the MP2RAGE sequence with an isotropic resolution of 0.75 mm^3.

The default coil combination provided on most MRI systems is generally not optimized for phase reconstruction, producing poor phase images with many spatial and temporal phase wraps. When performing phase regression, a quality phase image is needed to produce a proper fit between magnitude and phase data. To improve the phase

images, we used a coil combination with coil sensitivities estimated using singular value decomposition (SVD) for the reconstruction of the functional data [35]. This was beneficial for avoiding destructive interference between coils when reconstructing phase data. Instead of using a pre-scan as before [35], the coil sensitivity was estimated using an integrated SVD from the first 25 volumes of the current run before beginning the reconstruction. While this slightly delays the start of reconstruction, it generally does not delay the time to a completely reconstructed run, as the image reconstruction is faster than the acquisition. It also allows the coil sensitivities to be estimated for each run individually, making the approach robust against motion that may occur between runs. These coil sensitivities are now applied directly, and the reconstruction happens on the MRI system.

2.2.1.3   Visual Stimuli

Separate visual stimuli were used for the ODC and retinotopy functional imaging sessions. Both visual stimuli were created and presented in PsychoPy (v2021.2.0) [36] and spanned a total visual angle of approximately 40°, while the checkerboard spanned approximately the centre 20°. The ODC imaging stimulus consisted of a 10 Hz contrast reversing checkerboard on a grey background with a central fixation cross. It faded to grey at the periphery of the checkerboard to avoid any persistent contrasts in the outer portion of the stimulus. This was paired with goggles modified from the Portable Liquid crystal Apparatus for Tachistoscopic Occlusion (PLATO) Visual Occlusion Spectacles that use lenses made of liquid crystal cells [37]. The lenses can rapidly change from transparent to light-scattering independent of one another. These goggles were mounted on the occipital parietal RF coil between the participant's eyes and the mirror. The visual stimulus alternated between 30 seconds off and 30 seconds on for 10 repetitions. Each time the visual stimulus turned on, the goggles would change transparent and light-scattering lenses, rotating through three stimulation conditions of binocular, right eye, and left eye stimulation. The grey colour of the lenses when set to light-scattering was very similar to the background of the visual stimulus. A septum divider was also attached

to the front of the goggles to prevent excess light from the visual stimulus illuminating the opposing lens during monocular stimulation.

The timing of each lens changing opacity was controlled through PsychoPy, incorporated along with the visual stimulus timing. Measurement Computing's Universal Library was imported into PsychoPy and used to control a miniLAB 1008 USB data acquisition (DAQ) device. The DAQ provided two separate digital outputs to the controller of the goggles. Each digital output was used to control the opacity of a single lens, allowing for any of the four possible combinations of transparent and light-scattering lenses. Incorporating the DAQ programming into PsychoPy prevented any timing issues between the stimulus and goggles by controlling them simultaneously. The script used for controlling the stimulus and goggles is available publicly via GitHub: https://github.com/brettliem/phaseregression.git.

The second visual stimulus consisted of bowtie-shaped wedges that were portions of a 10 Hz contrast reversing checkerboard on a grey background with a central fixation cross. Each wedge subtended 45° extending from the central fixation cross and a bowtie was made up of two radially opposing wedges. The bowtie orientation alternated from vertical to horizontal every 18 seconds for 8 repetitions with an additional 18 second baseline at the beginning and end of the task. It has been demonstrated that this stimulus with a contrast of Vertical > Horizontal will highlight the boundaries of visual areas [38,39] and in the current study it was used to find the boundary between V1 and the secondary visual cortex (V2).

2.2.2   Data Preprocessing

2.2.2.1   Functional Data

The functional datasets from both the ODC and retinotopy imaging sessions underwent the same preprocessing. The magnitude data was motion corrected and aligned to the first volume of the first run using AFNI (22.0.11) [40]. Motion correction with AFNI provides the ability to save the transformations along with the six motion regressors. The

transformations from the magnitude data motion correction were applied to the corresponding phase data to motion correct and realign the phase data with the magnitude data.

The phase data from the coil combination using an SVD estimation of coil sensitivity has reduced spatial and temporal phase wraps and produced a smoother phase image [35]. However, to improve the quality of the phase data even further it still underwent additional spatial and temporal unwrapping using the Rapid Opensource Minimum spanning treE algOrithm (ROMEO) [41]. ROMEO provides fast and accurate exact phase unwrapping that can unwrap four dimensions in a single step, making it well suited for fMRI studies involving phase data.

Denoising the magnitude data was extremely important for phase regression as it improves the quality of the fit between the magnitude and phase data. Without any denoising at sub-millimeter resolutions, the fit between magnitude and phase data is heavily influenced by noise. In the first high-resolution study that used phase regression, Stanley et al. (2020) [33] used CompCor for removing physiological noise [42]. It has been shown that at sub-millimeter resolutions, thermal noise tends to dominate the magnitude data more than physiological noise [43]. Therefore, in the current study we used NOise Reduction with DIstribution Corrected (NORDIC) for thermal denoising as it is effective at removing noise without altering any desirable BOLD signal changes corresponding to neural activity [44].

Low frequency drifts caused by the scanner instabilities [45] can also appear in both the magnitude and phase data as a gradual increase or decrease over the course of the time series. This greatly affects the ability to fit magnitude and phase together as the amount of drift in the two quantities can be inconsistent. To remove the low frequency drifts, the magnitude and phase data were detrended using FSL FEAT preprocessing [46], using a high-pass filter of 0.01 Hz.

2.2.2.2   Phase Regression

In the current study, phase regression was performed using a custom MATLAB (2021b) script (https://github.com/brettliem/phaseregression.git) built upon previous work [25,27,33,47]. The script fits each corresponding voxel of magnitude and phase together linearly. A unified least-squared-error and maximum likelihood estimator was used for the fit [48]. This estimator considers the magnitude and phase time series along with the temporal standard error of each time series and calculates the correlation between the magnitude and phase time series to determine the best fit in each voxel. A high-pass filter of 0.15 Hz, which is above the task frequency, is used to estimate the temporal standard error in each of the magnitude and phase data. The fit parameters were then used to produce a maximum likelihood estimator of the amount of the magnitude signal fluctuations that could be accounted for by the phase fluctuations in a least-squared sense. This estimator (ascribed to the venous BOLD signal) is subtracted from the native magnitude time series to give a magnitude time series that is more specific to microvasculature. The script performs phase regression at every voxel to produce a modified magnitude dataset ('phase regressed") that is more specific to microvasculature and was performed on the data from the ODC session.

2.2.2.3   Structural Data

Presurfer [49] was used on the MP2RAGE images for bias field correction, background noise removal, and skull stripping the brain. This processed MP2RAGE image was then registered to the functional data using ANTs [50]. The scans from the retinotopy session were registered to the ODC session to avoid warping the ODC data as the columnar activation exists at a much finer resolution than that of the meridian mapping.

2.2.3   Data Analysis

Before performing phase regression, the quality of the preprocessed magnitude and phase data was determined by evaluating the temporal signal-to-noise ratio (tSNR) of the magnitude data and the temporal standard deviation of the phase data for each run. The

tSNR and temporal standard deviation maps were masked using the region-of-interest (ROI) that was used during all further analysis on each participant. These values were then averaged across runs and between participants to determine a single value for the study.

SPM 12 (Wellcome Department, UK) [51] was used for the general linear model (GLM) analysis of the unsmoothed native magnitude and phase regressed ODCs data, as well as the retinotopy data. The six motion regressors obtained from AFNI were converted to SPM format to be used as regressors in the GLM. This was done using a custom script (https://github.com/brettliem/phaseregression.git) that converts degrees to radians, reorders the motion regressors into the same sequence as used in SPM, divides the motion regressors back into their original runs and normalizes them about the first volume for each run. Voxels with t-values above 3.1 corresponding to an uncorrected significance level of $p < 0.001$ were identified as the activated regions for both the ODC and the retinotopy data.

2.2.3.1   ODCs on Inflated Surfaces

Cortical grey matter segmentation of the registered MP2RAGE was performed with the FreeSurfer recon-all pipeline [52,53]. The cortical segmentation was inspected to ensure accurate grey matter segmentation and manual corrections were performed when necessary. The Connectome Workbench [54] was used to register the activation maps on the inflated cortical surfaces. The Vertical > Horizontal contrast from retinotopy session (Figure 2.2), along with the Right > Left contrast from ODC session for both the native magnitude and phase regressed data were overlaid on the inflated surface (Figure 2.3). The Vertical > Horizontal contrast was used to localize V1 while the Right > Left contrast was used to show the sensitivity to a specific eye.

2.2.3.2   Laminar BOLD Signal Profiles

The functional data and registered MP2RAGE were upsampled in the in-plane resolution by a factor of four to provide smoother layering. For each participant, the location of the

ROI was determined using the Vertical > Horizontal contrast from their retinotopy images. The ROIs were manually drawn on ten slices to outline the white matter/grey matter (WM/GM) and grey matter/cerebrospinal fluid (GM/CSF) boundaries. Ten equidistant cortical layers were created in each ROI using LayNii (LN2_LAYERS) [55]. The mean and standard deviation of the BOLD signal changes produced during all three ocular stimulation conditions were calculated across each depth for both native magnitude and phase regressed data. These ten cortical layers are arbitrary and do not correspond directly to cortical layers I through VI, but the use of additional layers is beneficial when attempting to examine laminar differences and we will refer to the defined layers in three relatively even groups of superficial, middle, and deep cortical layers.

2.2.3.3   ODCs Across Cortical Depths

ODCs were examined across cortical depth in the same ROIs as the laminar BOLD signal profiles. Right- and left-eye-dominated columns were determined by thresholding the Right > Baseline and Left > Baseline maps at $t > 2.3$, respectively. Monocular stimulation of ODCs was compared across cortical depths to both binocular stimulation and monocular stimulation from the opposing eye. The mean and standard deviation of the BOLD signal changes were calculated in both right- and left-eye-dominated columns for all three ocular simulation conditions across each depth for both native magnitude and phase regressed data. Ratios were also calculated in ODCs across cortical depths between the conditions of ocular stimulation for both the native magnitude and phase regressed data to further compare right- and left-eye-dominated columns.

2.3   Results

An example of the native magnitude tSNR, phase regressed magnitude tSNR, and phase temporal standard deviation are displayed on a single brain slice in Figure 2.1. The phase temporal standard deviation was masked to avoid the high values outside of the brain. The native magnitude tSNR and phase temporal standard deviation were averaged within the ROI that was used for further analysis on each participant. The mean native

magnitude tSNR across participants was 20.91 ± 5.75 (mean $\pm$ standard deviation) and the mean phase temporal standard deviation was 0.020 ± 0.012 radians. After phase regression, the mean magnitude tSNR across participants was 19.94 ± 4.82.
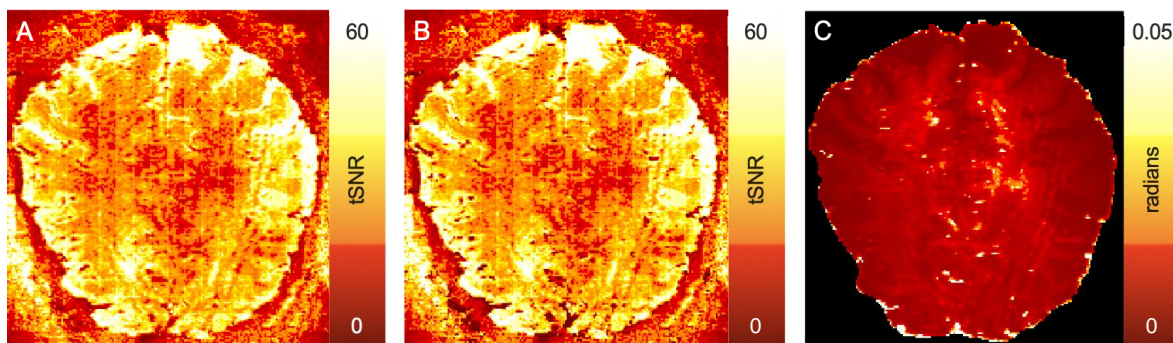
Figure 2.1. Data Quality. An example slice from tSNR maps of the A) native magnitude and B) phase regressed data, along with the C) phase temporal standard deviation.

Before we examined the BOLD signal specificity in ODCs with phase regression, we needed to precisely localize V1. Meridian mapping from the retinotopy session was used to determine the boundaries of the visual areas. Figure 2.2 illustrates the Vertical > Horizontal activation map from a single participant overlaid on the inflated cortical surface from their left hemisphere. The black lines marked the boundaries of the visual areas, as they followed the peak activation which should form a linear ridge down the centre of each region of activation. The three boundaries of particular interest were the V1/V2 dorsal boundary, the V1/V2 ventral boundary, and the V1 dorsal/ventral boundary. The V1 dorsal/ventral boundary was defined as the cool colour in the centre of all the areas of activation and provided the starting point for determining the location of the other boundaries. The V1/V2 dorsal and ventral boundaries are the closest boundary on either side of the V1 dorsal/ventral boundary. This clearly defined the location of V1 in each participant and was used as an aid when drawing the ROIs.
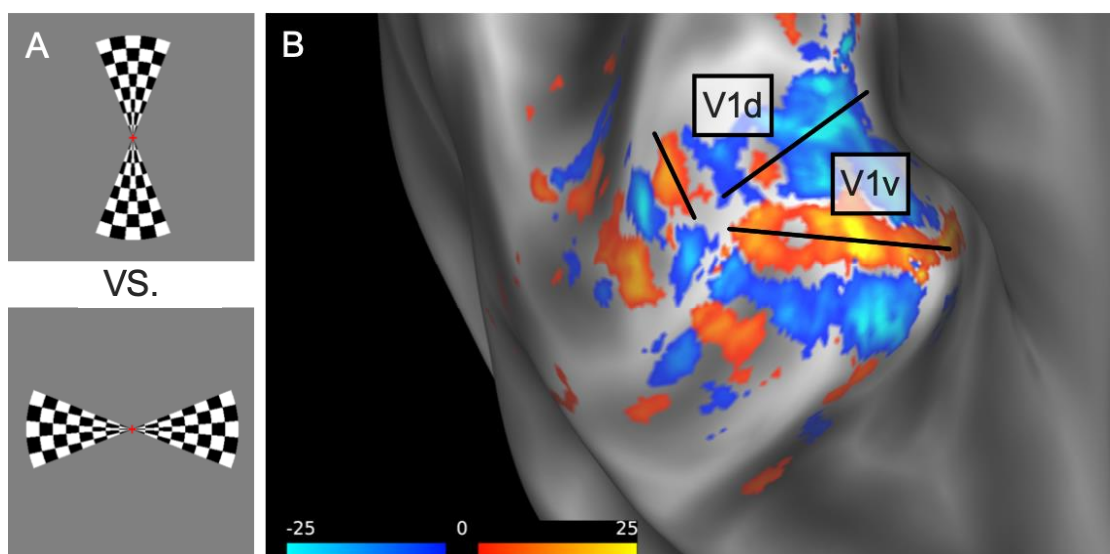
Figure 2.2. Retinotopic Meridian Mapping. A) The vertical and horizontal bowtie-shaped visual stimulus used for the meridian mapping. B) The activation map of the Vertical > Horizontal contrast from the native magnitude data of a single participant on the inflated cortical surface from their left hemisphere. The cool colours correspond to the vertical bowtie while the warm colours correspond to the horizontal bowtie.

The ODCs activation map (Right > Left) for native magnitude, phase regressed data and the absolute difference map between the two (areas of venous suppression) from the same participant were displayed using the same inflated cortical surface as in Figure 2.2 (Figure 2.3). It was important to ensure that ODCs were visible across V1 before moving to examine them laminarly. The results highlighted areas of the cortex that were predominantly sensitive to the input from one eye over the other. This revealed an alternating pattern of ODCs in V1, similar to those shown in previous fMRI studies [4,9,10]. Sensitivity to right and left monocular stimulation alternated in a blotchy stripe-like pattern across the cortex. Some signal remained outside the boundaries of V1 in other visual areas, although the amplitude of the signal was lower compared to V1. The absolute difference map between native magnitude and phase regressed ODCs showed widespread venous suppression across V1, within and outside of ODCs.
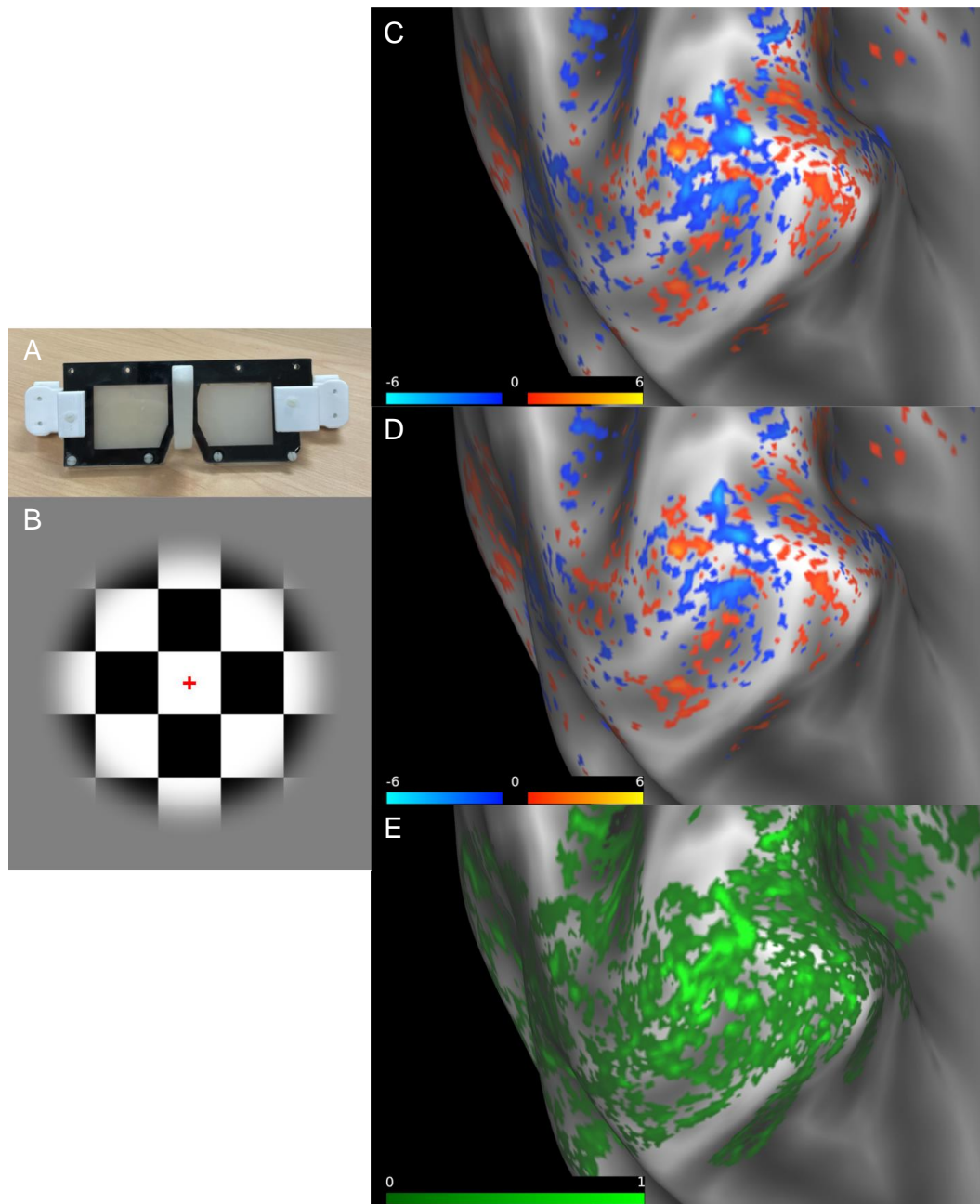
Figure 2.3. Ocular Dominance Columns fMRI Map. A) The goggles used to control which eye(s) could view the B) visual stimulus. The activation map of the Right > Left contrast of the C) native magnitude and the D) phase regressed data, overlaid on the inflated cortical surface from the left hemisphere of a single participant. The warm colours correspond to the sensitivity to right eye stimulation and the cool colours correspond to the sensitivity to left eye stimulation. E) The absolute difference map between the native magnitude and phase regressed data shows the areas of venous suppression.

To compare the spatial specificity of the depth-dependent BOLD signal with and without the phase regression, we performed a laminar analysis across V1. An example of ten cortical layers on a slice from a single participant is shown in Figure 2.4, along with the mean percent BOLD signal change in the ROI across the cortical depths during all three stimulation conditions in the native magnitude and phase regressed data. Right eye stimulation appeared to produce slightly greater BOLD signal changes than left eye stimulation across all cortical depths in the ROI. The native magnitude BOLD signal change at the most superficial cortical layer towards the CSF was approximately 2.8 times higher than in the deepest layer adjacent to the WM during binocular stimulation. During right and left eye stimulation, the most superficial layer was approximately 3.1 and 3.0 times higher than the deepest layer, respectively. Phase regression essentially removed the BOLD signal bias towards the cortical surface, with most superficial layer now only being approximately 1.2 times that of the deepest layer during binocular stimulation, and approximately 1.3 times higher during each monocular stimulation condition, which consequently lowered the tSNR of the image.
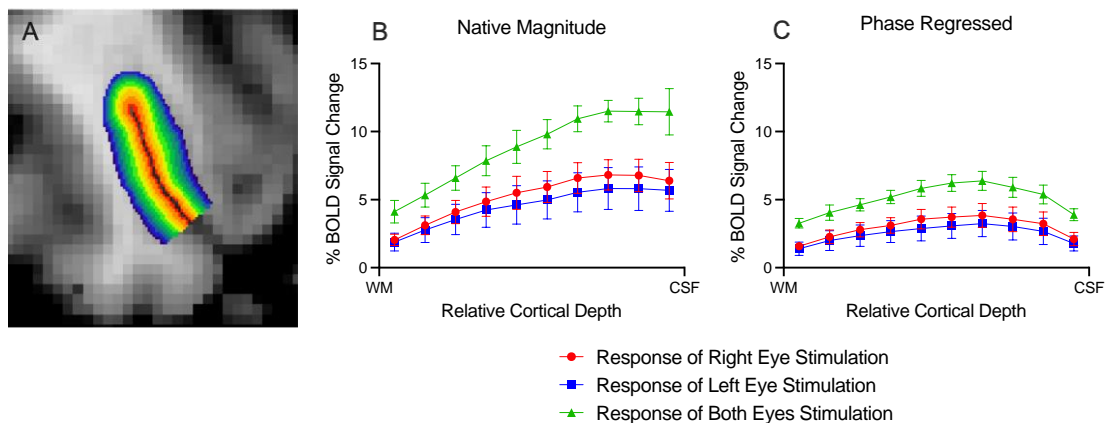
Figure 2.4. Laminar Profiles Across Cortical Depths. A) An example ROI of ten layers created for the analysis using LayNii. B) The native magnitude and C) phase regressed percent BOLD signal change across ten cortical depths corresponding to each stimulation condition. The error bars represent the standard error of the mean across participants.

The amount of venous suppression in V1, or the ratio between the percent BOLD signal change of the native magnitude and phase regressed data varied with cortical depth. Suppression ratios were calculated between native magnitude and phase regressed data for the binocular and monocular cases. As one approached the cortical surface, a greater ratio between the BOLD signal changes in the native magnitude and phase regressed data was observed, consistent with the preponderance and location of the venous vasculature (Figure 2.5).
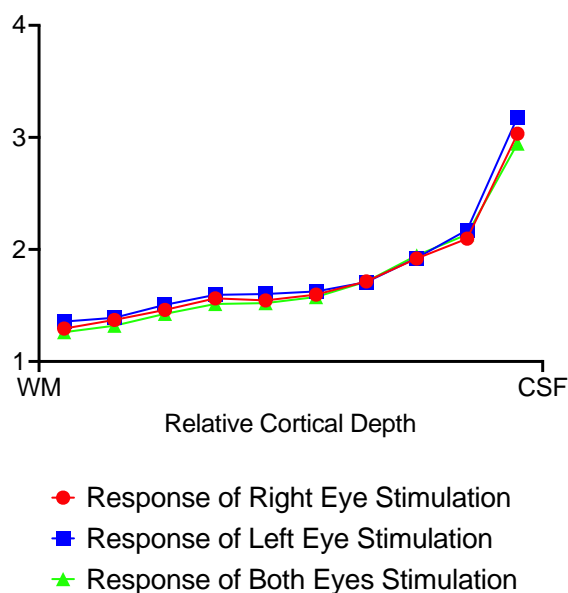
Figure 2.5. Suppression Ratios. The ratio between native magnitude and phase regressed data during each stimulation condition.

We also wanted to examine the laminar BOLD signal changes specifically within ODCs. This was done using the previously defined right- and left-eye-dominated columns. The percent BOLD signal change across cortical depths in ODCs produced by monocular and binocular stimulation for both the native magnitude and phase regressed data is shown in Figure 2.6. Both binocular and monocular stimulation produced a similar shaped laminar BOLD profile in ODCs as in the V1 ROI analysis above, which was expected as ODCs are restricted to V1. The amplitude of the BOLD signal changes

produced within the monocularly-defined columns were greater during binocular stimulation than monocular stimulation.
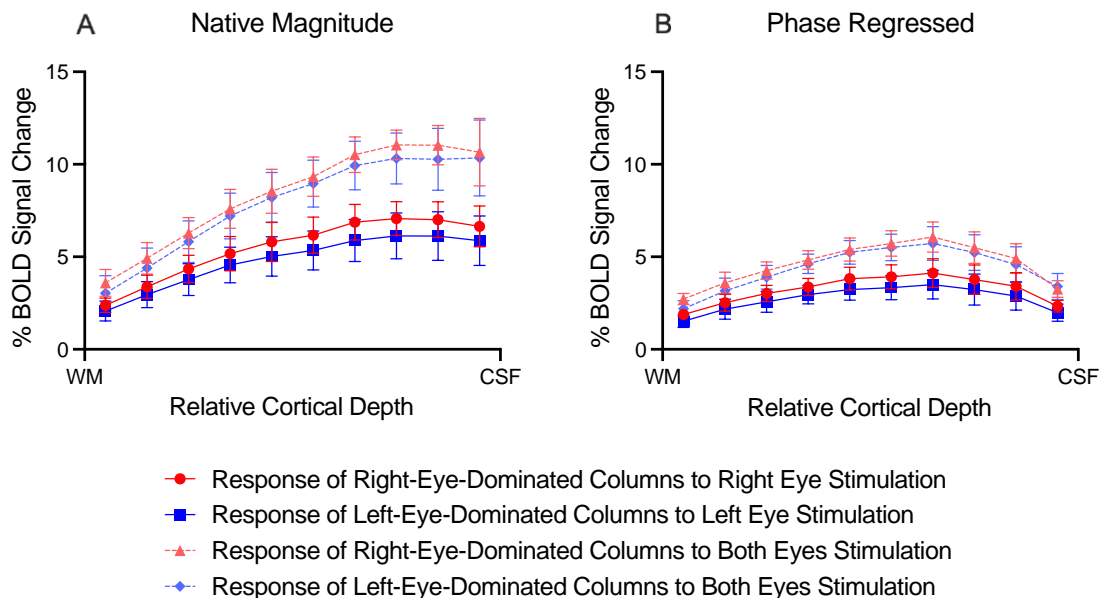
Figure 2.6. Binocular Stimulation in ODCs Across Cortical Depths. A) The native magnitude and B) phase regressed responses to monocular (solid lines) and binocular stimulation (dashed lines) in ODCs. The error bars represent the standard error of the mean across participants.

To investigate the differences produced by varying stimulation conditions in ODCs, ratios were taken between binocular and monocular stimulation (Figure 2.7). Binocular stimulation in ODCs produced 1.4-1.8 times the percent BOLD signal changes of monocular stimulation in both the native magnitude and phase regressed data. In left-eye-dominated columns, the ratio between binocular and monocular stimulation was consistently higher than in right-eye-dominated columns, except at the deepest cortical depth. Further examining the ratios, we see that the greatest difference between binocular stimulation and monocular stimulation in ODCs in the native magnitude data was at the most superficial cortical layers, while phase regression moved this more towards the middle cortical depth.
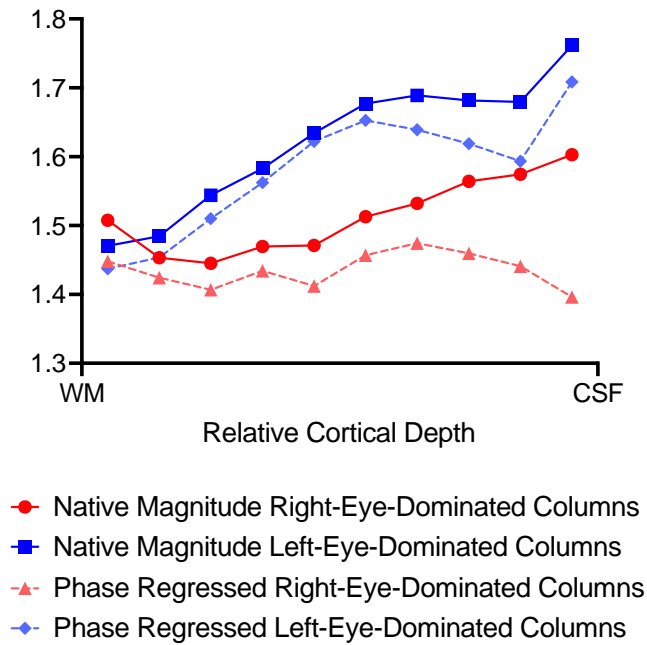
Figure 2.7. Ratios Between Binocular and Monocular Stimulation in ODCs. The ratios in ODCs between binocular and monocular stimulation that corresponds to the eye-dominated column for both the native magnitude (solid lines) and phase regressed (dashed lines) data.

The percent BOLD signal change across cortical depths in ODCs was presented again, but this time it showed the signal change produced in ODCs with corresponding and opposing monocular stimulation (Figure 2.8). Surprisingly, right and left monocular stimulation produced a very similar percent BOLD signal change regardless of stimulating a right- or left-eye-dominated column.
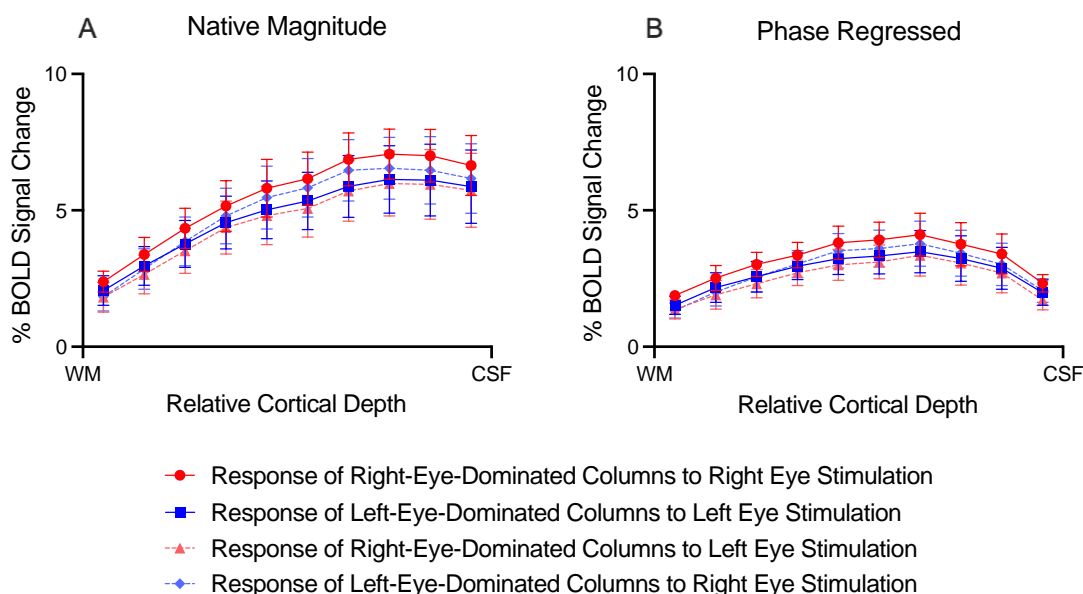
Figure 2.8. Opposing Monocular Stimulation in ODCs Across Cortical Depths. A) The native magnitude and B) phase regressed responses to corresponding monocular (solid lines) and opposing monocular (dashed lines) stimulation in ODCs. The error bars represent the standard error of the mean across participants.

Ratios were also taken in ODCs between corresponding and opposing monocular stimulation across cortical depths (Figure 2.9). The ratios clearly showed that in right-eye-dominated columns, right eye stimulation produced a greater percent BOLD signal change, represented by the ratio above 1.0. While in left-eye-dominated columns, right eye stimulation still produced a slightly greater percent BOLD signal change, represented by the ratio slightly below 1.0, aside from the deep cortical layers. The largest difference in BOLD signal change produced between corresponding and opposing monocular stimulation in ODCs was in the deep cortical layers.
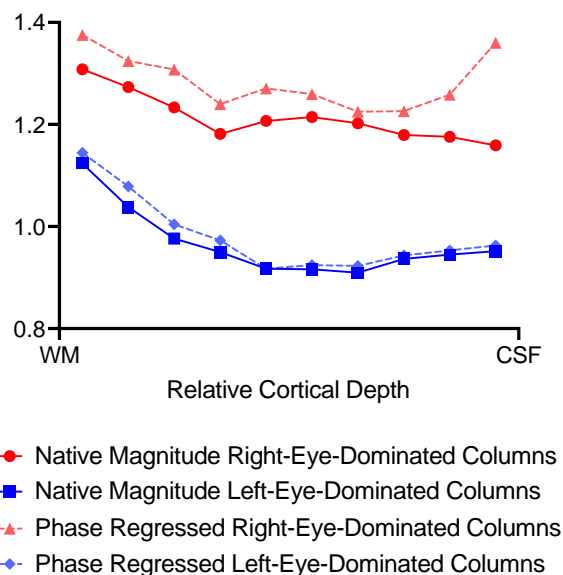
Figure 2.9. Ratios Between Opposing Monocular Stimulation in ODCs. The ratios in ODCs between corresponding and opposing monocular stimulation for both the native magnitude (solid lines) and phase regressed (dashed lines) data.

2.4   Discussion

In the current study, we examined the signal spatial specificity of the GRE BOLD contrast with and without the phase regression on the scale of cortical layers and columns of the human V1. Specifically, we expected the middle cortical depth of V1 to display the strongest differentiation between opposing ODCs, along with the peak in the laminar BOLD signal profile. Using GE-EPI, we performed retinotopic meridian mapping to locate V1 and imaged ODCs consecutively for each participant. The results showed improved laminar signal specificity with the phase regressed BOLD contrast compared to the native magnitude BOLD contrast, while failing to provide the signal specificity required within the cortex to accurately examine mesoscopic cortical structures. The results confirmed that phase regression is especially beneficial for high-resolution imaging when one is interested in investigating the BOLD signal change as a function of the cortical depth but has limitations when trying to distinguish adjacent columnar structures.

We performed similar retinotopic meridian mapping as performed by Greenberg et al. (2012) [38], but with an improved sub-millimeter imaging resolution at 7 T. The V1 areas between the boundaries shown in Figure 2.2 were used as an aid when drawing the ROIs to ensure the laminar analysis was restricted to V1. ODC data was displayed on an inflated surface (Figure 2.3), and it formed an alternating pattern of right and left eye preference in both the native magnitude and phase regressed data. This pattern of ODCs closely resemble those shown previously in humans with post-mortem histology and fMRI [8,10,11,56–60]. The areas with the greatest amount of venous suppression were aligned with the areas in the native magnitude ODC map that produced the largest BOLD signal changes. This was expected because the maximum signal changes seen in GRE BOLD are produced by large veins [15], as blood pools in principal intracortical veins from the surrounding microvasculature in areas of neural activity [18]. There was also venous suppression at the edges of adjacent ODCs which, on the phase regressed ODC map, made adjacent ODCs appear more distinct. This suggested that phase regression effectively suppressed BOLD signal changes distant from areas of neural activity [61]. Once referencing Figure 2.5, we assumed that this was achieved by suppressing the BOLD signal changes produced by pial veins, as they run along the cortical surface in the most superficial cortical layer. ODCs have been imaged previously using the BOLD contrast without phase regression [9–11], but in the current study it was demonstrated that phase regression suppressed BOLD signal changes distant from neural activity produced by pial surface veins [18,61] and reduced the amount of signal blurring between opposing ODCs.

BOLD signal profiles seen in most laminar fMRI studies typically have a similar shape to that of the native magnitude data shown in Figure 2.4 [4,21,23,62–75]. This is because the volume and density of large veins is skewed towards the cortical surface and their influence on the BOLD signal [18]. The middle cortical depths have the highest density of microvasculature and the highest metabolic rate [76,77], so we might expect to see the maximum signal change at the middle cortical depth (layer IVC). Some of the other most common acquisition techniques mentioned before, such as SE-EPI [21] and

VASO [22], provide this laminar signal profile by avoiding signal produced by large veins, but they suffer from a lower SNR and temporal resolution while being SAR-intensive [21,22]. A recent study by Hollander et al. (2021) [4] examined cortical depth-dependent BOLD signal in ODCs using a laminar deconvolution model for venous suppression developed by Markuerkiaga et al. (2016) [16]. They showed a laminar BOLD signal profile with a peak in the middle of the cortex within ODCs. Our results with phase regression were similar and we obtained a peak in the middle of the cortex within both V1 (Figure 2.4) and specific ODCs (Figure 2.6 and Figure 2.8). We also wanted to determine if phase regression was accurately suppressing BOLD signal changes by comparing the amount of suppression with the known organization of cortical vasculature. The blood volume density of principal intracortical veins increases approximately linearly approaching the cortical surface [16,76] and the suppression ratios we found in V1 (Figure 2.5) generally agree with this. However, our suppression ratios seemed to be slightly more exponential, rather than linear, particularly in the superficial cortical layers. Additionally, the peak in the phase regressed laminar BOLD signal profile appeared to be located somewhat more superficially rather than directly in the middle of the cortex. It has been previously shown that with the observed phase noise floor, EPI is unlikely to be sensitive to discrete phase changes from vessels below 150 µm in diameter [47], which would comprise the smaller principal intracortical veins, intracortical veins running parallel to the cortical surface, and microvasculature [76]. The diameter of principal intracortical veins increase up to a vessel diameter of approximately 170 µm as they approach the cortical surface [76] due blood pooling from microvasculature [18], which leaves only the most superficial principal intracortical veins and pial surface veins as vasculature producing measurable discrete phase changes [47]. This could be why the laminar profile peak was slightly more superficial than expected, as we are only obtaining sufficient phase information at the most superficial cortical depths which leads to inadequate intracortical venous suppression.

When examining the response in ODCs across cortical depths, we first noticed that BOLD signal changes produced across all cortical depths within the monocularly-

defined columns were greater during binocular stimulation than monocular stimulation (Figure 2.6). Hubel and Wiesel (1962) [7] showed that there are varying amounts of interaction between ODCs above and below layer IVC. Outside of layer IVC, ODCs can vary from being sensitive to input exclusively from one eye or from both eyes equally [7]. This could be why, in the current study, binocular stimulation produced greater BOLD signal changes than monocular stimulation, even in monocularly-defined columns. We attempted to further examine this using depth-dependent ratios between binocular and monocular stimulation in ODCs (Figure 2.7). Although the ratios in left-eye-dominated columns were greater than in right-eye-dominated columns, the native magnitude ratios in both monocularly-defined columns had similar trends with a slight peak in the deep cortical layers and a general increase approaching the cortical surface. The similarities continued between the phase regressed ratios, both showing slight suppression in the superficial cortical layers and the only main difference between the two being in the most superficial layer, where the ratio in the left-eye-dominated column did not continue decreasing. If the ratios significantly decreased at more superficial cortical layers with phase regression, we might assume that the increased BOLD signal changes found during binocular stimulation were due to local neural activity, as the increased BOLD signal changes in the superficial cortical layers during binocular stimulation would not have been suppressed with phase regression. In contrast, if the ratios remained similar to that of the native magnitude, we might assume the increased BOLD signal changes during binocular stimulation were due to additional blood pooling in primary intracortical veins because of increased neural activity in layer IVC from stimulating adjacent ODCs, as the increased BOLD signal changes in the superficial layers during binocular stimulation would have been suppressed with phase regression. Our results landed somewhere in between, which suggested that the increased BOLD signal changes found in the superficial cortical layers during binocular stimulation might be a combination of both increased amounts neural activity from intercolumn interactions and more blood pooling in primary intracortical veins from the increased activity in layer IVC from stimulating adjacent ODCs.

We were expecting the signal specificity in ODCs during right and left eye stimulation to be most defined in layer IVC because this is where ODCs are exclusively sensitive to monocular stimulation [7]. For this reason, we also expected the ratios between corresponding and opposing monocular stimulation in the monocularly-defined columns to be much greater than one in the middle of the cortex. The monocularly-defined columns should be more sensitive to the corresponding monocular stimulation, so it was unexpected that the BOLD signal changes in ODCs with the corresponding and opposing monocular stimulation were nearly identical (Figure 2.8). This was also shown in Figure 2.9Figure 2.8 as the ratios were close to one, and phase regression was providing minimal improvements. This led us to assume that there was a significant amount of overlap between the right- and left-eye-dominated columns defined from the t-maps against a control grey condition (as opposed to being defined from Right > Left or Left > Right, as is commonly done). Intracortical veins can reach well below the size where we can obtain useful phase information [47], to approximately 20 µm in diameter at their smallest, branching off from primary intracortical veins and extending outwards parallel to the cortical surface [76]. Since they produce BOLD signal changes distant from areas of neural activity that could blur the vascular response between adjacent columns, this could have reduced our ability to accurately define right- and left-eye-dominated columns.

Across all our results, right eye stimulation produced slightly greater BOLD signal changes than left eye stimulation. This was most notable in Figure 2.9, as left-eye-dominated columns produced greater BOLD signal changes with right eye stimulation, except in the deep layers. Hubel and Wiesel (1977) [78] studied ODCs with early deprivation on the visual system in monkeys, and the ODCs corresponding to monocular stimulation appeared to take over area from the ODCs corresponding to monocular closure, which led to wider columns that respond to the stimulated eye. While most monocular deprivation studies were performed during development, it has also been shown that the eye preference of neurons in the upper and lower cortical layers of ODCs may change even after development [79]. Most humans preferentially use one eye over

the other (66% right eye, 24% left eye, 10% no preference) [80] and it was qualitatively shown by Goodyear et al. (2002) [59] that ODCs corresponding to the preferred eye are slightly wider. Slightly wider right-eye-dominated columns would mean that a larger portion of V1 is sensitive to right eye stimulation than left eye stimulation. This would correspond to more deoxygenated blood pooling in large veins and could be responsible for the slightly greater BOLD signal changes during right eye stimulation. The spatial resolution of the functional imaging in the current study could also have been responsible because we used a voxel size that is somewhat wider than the width of an ODC, as opposed to Goodyear et al. (2002) [59] who used an in-plane resolution slightly narrower than the width of an ODC. The partial volume effects between adjacent ODCs in the current study could have led to the larger response during right eye stimulation and the inability to separate the responses from right and left monocular stimulation. BOLD signal changes during right eye stimulation would have appeared in more voxels if the width of the right-eye-dominated ODCs were slightly larger than both the width of the left-eye dominated columns and the voxel size.

A limitation of the current study was our functional imaging resolution of 0.8 mm isotropic. This not only could have affected the ability to define ODCs as mentioned above, but also our ability to define cortical depths. The human visual cortex is one the most convoluted, myelinated, and thinner parts of the cortex, and 0.8 mm isotropic only provided approximately 2-3 voxels across the depth of V1. This resolution was relatively coarse compared to the depth and curvature of the cortex in V1, meaning that automated cortical segmentations were susceptible to partial volume errors. Our data was upsampled to minimize the number of these errors, but this also required manual correction of the cortical segmentation to avoid leaving entire voxels in the CSF or WM, and manual correction can be prone to error.

Another important limitation of the current study was that the use of partial Fourier in high-resolution fMRI has been shown to cause signal blurring [81]. Signal blurring can affect its specificity, which is important when examining sub-millimeter

cortical structures and could have influenced our ability to monocularly define columns. However, the more critical aspect of this limitation to discuss for the current study was phase blurring, as significant phase blurring between voxels with and without veins would affect the amount and location of venous suppression during phase regression. The improved quality of phase data produced by the phase sensitive coil combination should have reduced the significance of phase blurring, but the amount and effects of phase blurring caused by partial Fourier between voxels with and without veins should be further investigated.

An advantage to using GE-EPI with phase regression in laminar fMRI studies is that it can be collected with a higher temporal resolution than other techniques, as shown in the current study. GE-EPI is normally offset by its lower specificity to microvasculature, which is why alternate imaging sequences with greater spatial specificity and lower temporal resolutions are often employed in laminar fMRI studies. Phase regression is a data-driven method to improve the spatial specificity of GRE BOLD while maintaining its higher temporal resolution, which makes it possible to study functional connectivity between cortical layers.

2.5   Conclusions

GE-EPI with phase regression has been shown to be effective at suppressing the BOLD signal from pial vessels in high-resolution laminar analysis of the human brain at 7 T. Phase regression provides a simple approach for suppressing the unwanted BOLD signal from the large surface veins that typically dominates over the contribution from the microvasculature. The increased spatial specificity of this method provides a more accurate representation of laminar BOLD signal. However, phase regression does not improve the contrast between columns, suggesting that the phase is not sensitive to the venous vessel sizes running parallel to the cortical surface in the various layers. Phase regression provides data-driven suppression of large veins, as opposed to other methods requiring additional imaging or models of vasculature. Overall, GRE BOLD with phase

regression is promising for high-resolution laminar fMRI studies due to its straightforward method of removing the venous bias from the BOLD signal.

2.6 References

[1] J.H. Duyn, The future of ultra-high field MRI and fMRI for study of the human brain, Neuroimage. 62 (2012) 1241–1248. https://doi.org/10.1016/j.neuroimage.2011.10.065.

[2] C.A. Olman, N. Harel, D.A. Feinberg, S. He, P. Zhang, K. Ugurbil, E. Yacoub, Layer-Specific fMRI Reflects Different Neuronal Computations at Different Depths in Human V1, Plos One. 7 (2012) e32536. https://doi.org/10.1371/journal.pone.0032536.

[3] F.D. Martino, J. Zimmermann, L. Muckli, K. Ugurbil, E. Yacoub, R. Goebel, Cortical Depth Dependent Functional Responses in Humans at 7T: Improved Specificity with 3D GRASE, Plos One. 8 (2013) e60514. https://doi.org/10.1371/journal.pone.0060514.

[4] G. de Hollander, W. van der Zwaag, C. Qian, P. Zhang, T. Knapen, Ultra-high field fMRI reveals origins of feedforward and feedback activity within laminae of human ocular dominance columns, Neuroimage. 228 (2021) 117683. https://doi.org/10.1016/j.neuroimage.2020.117683.

[5] R.J. Douglas, K.A.C. Martin, Neuronal Circuits of the Neocortex, Neuroscience. 27 (2004) 419–451. https://doi.org/10.1146/annurev.neuro.27.070203.144152.

[6] M.W. Self, T. van Kerkoerle, R. Goebel, P.R. Roelfsema, Benchmarking laminar fMRI: Neuronal spiking and synaptic activity during top-down and bottom-up processing in the different layers of cortex, Neuroimage. 197 (2019) 806–817. https://doi.org/10.1016/j.neuroimage.2017.06.045.

[7] D.H. Hubel, T.N. Wiesel, Receptive fields, binocular interaction and functional architecture in the cat's visual cortex, J Physiology. 160 (1962) 106–154. https://doi.org/10.1113/jphysiol.1962.sp006837.

[8] J.C. Horton, L.R. Dagi, E.P. McCrane, F.M. de Monasterio, Arrangement of Ocular Dominance Columns in Human Visual Cortex, Arch Ophthalmol-Chic. 108 (1990) 1025–1031. https://doi.org/10.1001/archopht.1990.01070090127054.

[9] R.S. Menon, S. Ogawa, J.P. Strupp, K. Uğurbil, Ocular Dominance in Human V1 Demonstrated by Functional Magnetic Resonance Imaging, J Neurophysiol. 77 (1997) 2780–2787. https://doi.org/10.1152/jn.1997.77.5.2780.

[10] K. Cheng, R.A. Waggoner, K. Tanaka, Human Ocular Dominance Columns as Revealed by High-Field Functional Magnetic Resonance Imaging, Neuron. 32 (2001) 359–374. https://doi.org/10.1016/s0896-6273(01)00477-9.

[11] E. Yacoub, A. Shmuel, N. Logothetis, K. Uğurbil, Robust detection of ocular dominance columns in humans using Hahn Spin Echo BOLD functional MRI at 7 Tesla, Neuroimage. 37 (2007) 1161–1177. https://doi.org/10.1016/j.neuroimage.2007.05.020.

[12] S. Ogawa, T.M. Lee, A.R. Kay, D.W. Tank, Brain magnetic resonance imaging with contrast dependent on blood oxygenation., Proc National Acad Sci. 87 (1990) 9868–9872. https://doi.org/10.1073/pnas.87.24.9868.

[13] S. Ogawa, T. Lee, A.S. Nayak, P. Glynn, Oxygenation-sensitive contrast in magnetic resonance image of rodent brain at high magnetic fields, Magnet Reson Med. 14 (1990) 68–78. https://doi.org/10.1002/mrm.1910140108.

[14] R.S. Menon, The great brain versus vein debate, Neuroimage. 62 (2012) 970–974. https://doi.org/10.1016/j.neuroimage.2011.09.005.

[15] S. Ogawa, R.S. Menon, D.W. Tank, S.G. Kim, H. Merkle, J.M. Ellermann, K. Ugurbil, Functional brain mapping by blood oxygenation level-dependent contrast magnetic resonance imaging. A comparison of signal characteristics with a biophysical model, Biophys J. 64 (1993) 803–812. https://doi.org/10.1016/s0006-3495(93)81441-3.

[16] I. Markuerkiaga, M. Barth, D.G. Norris, A cortical vascular model for examining the specificity of the laminar BOLD signal, Neuroimage. 132 (2016) 491–498. https://doi.org/10.1016/j.neuroimage.2016.02.073.

[17] K. Uludağ, P. Blinder, Linking brain vascular physiology to hemodynamic response in ultra-high field MRI, Neuroimage. 168 (2018) 279–295. https://doi.org/10.1016/j.neuroimage.2017.02.063.

[18] R. Turner, How Much Cortex Can a Vein Drain? Downstream Dilution of Activation-Related Cerebral Blood Oxygenation Changes, Neuroimage. 16 (2002) 1062–1067. https://doi.org/10.1006/nimg.2002.1082.

[19] S.-G. Kim, S. Ogawa, Biophysical and Physiological Origins of Blood Oxygenation Level-Dependent fMRI Signals, J Cereb Blood Flow Metabolism. 32 (2012) 1188–1206. https://doi.org/10.1038/jcbfm.2012.23.

[20] K. Kay, K.W. Jamison, L. Vizioli, R. Zhang, E. Margalit, K. Ugurbil, A critical assessment of data quality and venous effects in sub-millimeter fMRI, Neuroimage. 189 (2019) 847–869. https://doi.org/10.1016/j.neuroimage.2019.02.006.

[21] J.B.M. Goense, N.K. Logothetis, Laminar specificity in monkey V1 using high-resolution SE-fMRI, Magn Reson Imaging. 24 (2006) 381–392. https://doi.org/10.1016/j.mri.2005.12.032.

[22] H. Lu, X. Golay, J.J. Pekar, P.C.M. van Zijl, Functional magnetic resonance imaging based on changes in vascular space occupancy, Magnet Reson Med. 50 (2003) 263–274. https://doi.org/10.1002/mrm.10519.

[23] J.R. Polimeni, B. Fischl, D.N. Greve, L.L. Wald, Laminar analysis of 7T BOLD using an imposed spatial activation pattern in human V1, Neuroimage. 52 (2010) 1334–1346. https://doi.org/10.1016/j.neuroimage.2010.05.005.

[24] J.C.W. Siero, J. Hendrikse, H. Hoogduin, N. Petridou, P. Luijten, M.J. Donahue, Cortical depth dependence of the BOLD initial dip and poststimulus undershoot in human visual cortex at 7 Tesla, Magnet Reson Med. 73 (2015) 2283–2295. https://doi.org/10.1002/mrm.25349.

[25] R.S. Menon, Postacquisition suppression of large-vessel BOLD signals in high-resolution fMRI, Magnet Reson Med. 47 (2002) 1–9. https://doi.org/10.1002/mrm.10041.

[26] R.L. Barry, J.C. Gore, Enhanced phase regression with savitzky-golay filtering for high-resolution BOLD fMRI, Hum Brain Mapp. 35 (2014) 3832–3840. https://doi.org/10.1002/hbm.22440.

[27] A.T. Curtis, R.M. Hutchison, R.S. Menon, Phase based venous suppression in resting-state BOLD GE-fMRI, Neuroimage. 100 (2014) 51–59. https://doi.org/10.1016/j.neuroimage.2014.05.079.

[28] R.L. Barry, J.M. Williams, L.M. Klassen, J.P. Gallivan, J.C. Culham, R.S. Menon, Evaluation of preprocessing steps to compensate for magnetic field distortions due to body movements in BOLD fMRI, Magn Reson Imaging. 28 (2010) 235–244. https://doi.org/10.1016/j.mri.2009.07.005.

[29] R.L. Barry, S.C. Strother, J.C. Gore, Complex and magnitude-only preprocessing of 2D and 3D BOLD fMRI data at 7 T, Magnet Reson Med. 67 (2012) 867–871. https://doi.org/10.1002/mrm.23072.

[30] R.E. Martin, B.J. MacIntosh, R.C. Smith, A.M. Barr, T.K. Stevens, J.S. Gati, R.S. Menon, Cerebral Areas Processing Swallowing and Tongue Movement Are Overlapping but Distinct: A Functional Magnetic Resonance Imaging Study, J Neurophysiol. 92 (2004) 2428–2443. https://doi.org/10.1152/jn.01144.2003.

[31] D.B. Rowe, C.P. Meller, R.G. Hoffmann, Characterizing phase-only fMRI data with an angular regression model, J Neurosci Meth. 161 (2007) 331–341. https://doi.org/10.1016/j.jneumeth.2006.10.024.

[32] D.G. Tomasi, E.C. Caparelli, Macrovascular Contribution in Activation Patterns of Working Memory, J Cereb Blood Flow Metabolism. 27 (2006) 33–42. https://doi.org/10.1038/sj.jcbfm.9600314.

[33] O.W. Stanley, A.B. Kuurstra, L.M. Klassen, R.S. Menon, J.S. Gati, Effects of phase regression on high-resolution functional MRI of the primary visual cortex, Neuroimage. 227 (2021) 117631. https://doi.org/10.1016/j.neuroimage.2020.117631.

[34] K.M. Gilbert, J.S. Gati, R.S. Menon, Occipital-parietal coil with variable-density element distribution for 7T functional imaging, Proceedings of the 25th International Society for Magnetic Resonance in Medicine Annual Meeting. (2017). https://cds.ismrm.org/protected/17MProceedings/PDFfiles/4307.html.

[35] O.W. Stanley, R.S. Menon, L.M. Klassen, Receiver phase alignment using fitted SVD derived sensitivities from routine prescans, Plos One. 16 (2021) e0256700. https://doi.org/10.1371/journal.pone.0256700.

[36] J. Peirce, J.R. Gray, S. Simpson, M. MacAskill, R. Höchenberger, H. Sogo, E. Kastman, J.K. Lindeløv, PsychoPy2: Experiments in behavior made easy, Behav Res Methods. 51 (2019) 195–203. https://doi.org/10.3758/s13428-018-01193-y.

[37] P. Milgram, A spectacle-mounted liquid-crystal tachistoscope, Behav Res Methods Instruments Comput. 19 (1987) 449–456. https://doi.org/10.3758/bf03205613.

[38] A.S. Greenberg, T. Verstynen, Y.-C. Chiu, S. Yantis, W. Schneider, M. Behrmann, Visuotopic Cortical Connectivity Underlying Attention Revealed with White-Matter Tractography, J Neurosci. 32 (2012) 2773–2782. https://doi.org/10.1523/jneurosci.5419-11.2012.

[39] S.D. Slotnick, S. Yantis, Efficient acquisition of human retinotopic maps, Hum Brain Mapp. 18 (2003) 22–29. https://doi.org/10.1002/hbm.10077.

[40] R.W. Cox, AFNI: Software for Analysis and Visualization of Functional Magnetic Resonance Neuroimages, Comput Biomed Res. 29 (1996) 162–173. https://doi.org/10.1006/cbmr.1996.0014.

[41] B. Dymerska, K. Eckstein, B. Bachrata, B. Siow, S. Trattnig, K. Shmueli, S.D. Robinson, Phase unwrapping with a rapid opensource minimum spanning tree algorithm (ROMEO), Magnet Reson Med. 85 (2021) 2294–2308. https://doi.org/10.1002/mrm.28563.

[42] Y. Behzadi, K. Restom, J. Liau, T.T. Liu, A component based noise correction method (CompCor) for BOLD and perfusion based fMRI, Neuroimage. 37 (2007) 90–101. https://doi.org/10.1016/j.neuroimage.2007.04.042.

[43] C. Triantafyllou, R.D. Hoge, G. Krueger, C.J. Wiggins, A. Potthast, G.C. Wiggins, L.L. Wald, Comparison of physiological noise at 1.5 T, 3 T and 7 T and optimization of fMRI acquisition parameters, Neuroimage. 26 (2005) 243–250. https://doi.org/10.1016/j.neuroimage.2005.01.007.

[44] S. Moeller, P.K. Pisharady, S. Ramanna, C. Lenglet, X. Wu, L. Dowdle, E. Yacoub, K. Uğurbil, M. Akçakaya, NOise reduction with DIstribution Corrected (NORDIC) PCA in dMRI with complex-valued parameter-free locally low-rank processing, Neuroimage. 226 (2021) 117539. https://doi.org/10.1016/j.neuroimage.2020.117539.

[45] A.M. Smith, B.K. Lewis, U.E. Ruttimann, F.Q. Ye, T.M. Sinnwell, Y. Yang, J.H. Duyn, J.A. Frank, Investigation of Low Frequency Drift in fMRI Signal, Neuroimage. 9 (1999) 526–533. https://doi.org/10.1006/nimg.1999.0435.

[46] M. Jenkinson, C.F. Beckmann, T.E.J. Behrens, M.W. Woolrich, S.M. Smith, FSL, Neuroimage. 62 (2012) 782–790. https://doi.org/10.1016/j.neuroimage.2011.09.015.

[47] M. Klassen, R.S. Menon, BOLD Phase and Mag Dependance on Vessel Geometry, Proceedings of the 13th International Society for Magnetic Resonance in Medicine Annual Meeting. (2005).

[48] D. York, N.M. Evensen, M.L. Martínez, J.D.B. Delgado, Unified equations for the slope, intercept, and standard errors of the best straight line, Am J Phys. 72 (2004) 367–375. https://doi.org/10.1119/1.1632486.

[49] S. Kashyap, srikash/presurfer: ondu (1.0). Zenodo, (2021). https://doi.org/10.5281/zenodo.4626841.

[50] B.B. Avants, N.J. Tustison, G. Song, P.A. Cook, A. Klein, J.C. Gee, A reproducible evaluation of ANTs similarity metric performance in brain image registration, Neuroimage. 54 (2011) 2033–2044. https://doi.org/10.1016/j.neuroimage.2010.09.025.

[51] K.J. Friston, A.P. Holmes, K.J. Worsley, J. -P. Poline, C.D. Frith, R.S.J. Frackowiak, Statistical parametric maps in functional imaging: A general linear approach, Hum Brain Mapp. 2 (1994) 189–210. https://doi.org/10.1002/hbm.460020402.

[52] A.M. Dale, B. Fischl, M.I. Sereno, Cortical Surface-Based Analysis I. Segmentation and Surface Reconstruction, Neuroimage. 9 (1999) 179–194. https://doi.org/10.1006/nimg.1998.0395.

[53] B. Fischl, M.I. Sereno, A.M. Dale, Cortical Surface-Based Analysis II: Inflation, Flattening, and a Surface-Based Coordinate System, Neuroimage. 9 (1999) 195–207. https://doi.org/10.1006/nimg.1998.0396.

[54] D.S. Marcus, J. Harwell, T. Olsen, M. Hodge, M.F. Glasser, F. Prior, M. Jenkinson, T. Laumann, S.W. Curtiss, D.C.V. Essen, Informatics and Data Mining Tools and Strategies for the Human Connectome Project, Front Neuroinform. 5 (2011) 4. https://doi.org/10.3389/fninf.2011.00004.

[55] L. (Renzo) Huber, B.A. Poser, P.A. Bandettini, K. Arora, K. Wagstyl, S. Cho, J. Goense, N. Nothnagel, A.T. Morgan, J. van den Hurk, A.K. Müller, R.C. Reynolds, D.R. Glen, R. Goebel, O.F. Gulban, LayNii: A software suite for layer-fMRI, Neuroimage. 237 (2021) 118091. https://doi.org/10.1016/j.neuroimage.2021.118091.

[56] D.L. Adams, J.C. Horton, Ocular Dominance Columns: Enigmas and Challenges, Neurosci. 15 (2009) 62–77. https://doi.org/10.1177/1073858408327806.

[57] R.S. Menon, B.G. Goodyear, Submillimeter functional localization in human striate cortex using BOLD contrast at 4 Tesla: Implications for the vascular point-spread function, Magnet Reson Med. 41 (1999) 230–235. https://doi.org/10.1002/(sici)1522-2594(199902)41:2<230::aid-mrm3>3.0.co;2-o.

[58] B.G. Goodyear, R.S. Menon, Brief visual stimulation allows mapping of ocular dominance in visual cortex using fMRI, Hum Brain Mapp. 14 (2001) 210–217. https://doi.org/10.1002/hbm.1053.

[59] B.G. Goodyear, D.A. Nicolle, R.S. Menon, High resolution fMRI of ocular dominance columns within the visual cortex of human amblyopes, Strabismus. 10 (2002) 129–136. https://doi.org/10.1076/stra.10.2.129.8140.

[60] J.C. Horton, E.T. Hedley-Whyte, Mapping of cytochrome oxidase patches and ocular dominance columns in human visual cortex, Philosophical Transactions Royal Soc Lond B Biological Sci. 304 (1984) 255–272. https://doi.org/10.1098/rstb.1984.0022.

[61] C.A. Olman, S. Inati, D.J. Heeger, The effect of large veins on spatial localization with GE BOLD at 3 T: Displacement, not blurring, Neuroimage. 34 (2007) 1126–1135. https://doi.org/10.1016/j.neuroimage.2006.08.045.

[62] I. Markuerkiaga, J.P. Marques, T.E. Gallagher, D.G. Norris, Estimation of laminar BOLD activation profiles using deconvolution with a physiological point spread function, J Neurosci Meth. 353 (2021) 109095. https://doi.org/10.1016/j.jneumeth.2021.109095.

[63] J. Goense, H. Merkle, N.K. Logothetis, High-Resolution fMRI Reveals Laminar Differences in Neurovascular Coupling between Positive and Negative BOLD Responses, Neuron. 76 (2012) 629–639. https://doi.org/10.1016/j.neuron.2012.09.019.

[64] J. Goense, Y. Bohraus, N.K. Logothetis, fMRI at High Spatial Resolution: Implications for BOLD-Models, Front Comput Neurosc. 10 (2016) 66. https://doi.org/10.3389/fncom.2016.00066.

[65] L. Huber, J. Goense, A.J. Kennerley, R. Trampel, M. Guidi, E. Reimer, D. Ivanov, N. Neef, C.J. Gauthier, R. Turner, H.E. Möller, Cortical lamina-dependent blood volume changes in human brain at 7T, Neuroimage. 107 (2015) 23–33. https://doi.org/10.1016/j.neuroimage.2014.11.046.

[66] L. Huber, D.A. Handwerker, D.C. Jangraw, G. Chen, A. Hall, C. Stüber, J. Gonzalez-Castillo, D. Ivanov, S. Marrett, M. Guidi, J. Goense, B.A. Poser, P.A. Bandettini, High-Resolution CBV-fMRI Allows Mapping of Laminar Activity and Connectivity of Cortical Input and Output in Human M1, Neuron. 96 (2017) 1253-1263.e7. https://doi.org/10.1016/j.neuron.2017.11.005.

[67] L. Huber, D. Ivanov, D.A. Handwerker, S. Marrett, M. Guidi, K. Uludağ, P.A. Bandettini, B.A. Poser, Techniques for blood volume fMRI with VASO: From low-resolution mapping towards sub-millimeter layer-dependent applications, Neuroimage. 164 (2018) 131–143. https://doi.org/10.1016/j.neuroimage.2016.11.039.

[68] S. Kashyap, D. Ivanov, M. Havlicek, L. Huber, B.A. Poser, K. Uludağ, Sub-millimetre resolution laminar fMRI using Arterial Spin Labelling in humans at 7 T, Plos One. 16 (2021) e0250504. https://doi.org/10.1371/journal.pone.0250504.

[69] S. Kashyap, D. Ivanov, M. Havlicek, S. Sengupta, B.A. Poser, K. Uludağ, Resolving laminar activation in human V1 using ultra-high spatial resolution fMRI at 7T, Sci Rep-Uk. 8 (2018) 17063. https://doi.org/10.1038/s41598-018-35333-3.

[70] M. Moerel, F.D. Martino, V.G. Kemper, S. Schmitter, A.T. Vu, K. Uğurbil, E. Formisano, E. Yacoub, Sensitivity and specificity considerations for fMRI encoding, decoding, and mapping of auditory cortex at ultra-high field, Neuroimage. 164 (2018) 18–31. https://doi.org/10.1016/j.neuroimage.2017.03.063.

[71] J.C. Siero, N. Petridou, H. Hoogduin, P.R. Luijten, N.F. Ramsey, Cortical Depth-Dependent Temporal Dynamics of the BOLD Response in the Human Brain, J Cereb Blood Flow Metabolism. 31 (2011) 1999–2008. https://doi.org/10.1038/jcbfm.2011.57.

[72] J.H. Kim, D. Ress, Reliability of the depth-dependent high-resolution BOLD hemodynamic response in human visual cortex and vicinity, Magn Reson Imaging. 39 (2017) 53–63. https://doi.org/10.1016/j.mri.2017.01.019.

[73] A. Akbari, S. Bollmann, T.S. Ali, M. Barth, Modelling the depth-dependent VASO and BOLD responses in human primary visual cortex, Biorxiv. (2021) 2021.05.07.443052. https://doi.org/10.1101/2021.05.07.443052.

[74] L. Huber, E.S. Finn, Y. Chai, R. Goebel, R. Stirnberg, T. Stöcker, S. Marrett, K. Uludag, S.G. Kim, S. Han, P.A. Bandettini, B.A. Poser, Layer-dependent functional connectivity methods, Prog Neurobiol. (2020) 101835. https://doi.org/10.1016/j.pneurobio.2020.101835.

[75] W. Schellekens, A.A. Bhogal, E.C.A. Roefs, M.G. Báez-Yáñez, J.C.W. Siero, N. Petridou, The many layers of BOLD. On the contribution of different vascular compartments to laminar fMRI, Biorxiv. (2021) 2021.10.21.465359. https://doi.org/10.1101/2021.10.21.465359.

[76] H.M. Duvernoy, S. Delon, J.L. Vannson, Cortical blood vessels of the human brain, Brain Res Bull. 7 (1981) 519–579. https://doi.org/10.1016/0361-9230(81)90007-1.

[77] B. Weber, A.L. Keller, J. Reichold, N.K. Logothetis, The Microvascular System of the Striate and Extrastriate Visual Cortex of the Macaque, Cereb Cortex. 18 (2008) 2318–2330. https://doi.org/10.1093/cercor/bhm259.

[78] D.H. Hubel, T.N. Wiesel, Ferrier lecture - Functional architecture of macaque monkey visual cortex, Proc Royal Soc Lond Ser B Biological Sci. 198 (1977) 1–59. https://doi.org/10.1098/rspb.1977.0085.

[79] S. LeVay, T.N. Wiesel, D.H. Hubel, The development of ocular dominance columns in normal and visually deprived monkeys, J Comp Neurol. 191 (1980) 1–51. https://doi.org/10.1002/cne.901910102.

[80] M. Reiss, G. Reiss, Ocular Dominance: Some Family Data, Laterality. 2 (1997) 7–16. https://doi.org/10.1080/713754254.

[81] A.T. Vu, K. Jamison, M.F. Glasser, S.M. Smith, T. Coalson, S. Moeller, E.J. Auerbach, K. Uğurbil, E. Yacoub, Tradeoffs in pushing the spatial resolution of fMRI for the 7T Human Connectome Project, Neuroimage. 154 (2017) 23–32. https://doi.org/10.1016/j.neuroimage.2016.11.049.

Chapter 3

3   Conclusions and Future Directions

3.1   Summary

Phase regression is a valuable method that uses the routinely discarded phase data collected with GRE BOLD to reduce the large vein bias from the BOLD signal and increase the spatial specificity of conventional fMRI. The work presented in this thesis represents the first time both laminar and columnar analyses were performed on phase regressed GRE BOLD data. This thesis contributes to high-resolution fMRI studies by demonstrating that phase regression makes GRE BOLD better suited for laminar analyses, while also determining its limitations.

Chapter 2 of this thesis explored the efficacy of GRE BOLD with phase regression as a correction technique for laminar and columnar analyses in high-resolution fMRI studies by comparing the BOLD signal in both native magnitude and phase regressed data across cortical layers of ODCs. To accomplish this, GE-EPI data at 0.8 mm isotropic was collected from five participants in two functional imaging sessions, each using separate visual stimuli. The first imaging session consisted of retinotopic meridian mapping to localize for V1, and the second imaging session used custom goggles that could provide monocular or binocular vision paired with the visual stimulus to image ODCs. Phase regression suppressed BOLD signal changes distant from neural activity produced by pial surface veins [1,2], which reduced the amount of signal blurring between opposing ODCs when displayed on an inflated surface. The native magnitude and phase regressed data were compared in V1 across cortical layers using laminar BOLD signal profiles. While the native magnitude BOLD signal increased towards the cortical surface, the phase regressed BOLD signal showed a peak near the middle cortical depth. This corresponded more to the density of microvasculature without the venous bias [3]. ODCs were also examined across cortical depths by comparing laminar BOLD signal profiles of right- and left-eye-dominated columns with varying stimulation

conditions. Binocular stimulation was shown to produce greater BOLD signal changes in ODCs than monocular stimulation, which could be a result of both additional intercolumn interactions and increased blood pooling in principal intracortical veins from the adjacent ODCs during binocular stimulation. When comparing corresponding and opposing monocular stimulation, the BOLD signal changes were nearly equal. This was consistent for the native magnitude and phase regressed data, which suggested that there was a significant amount of overlap between the right- and left-eye-dominated columns defined with monocular stimulation. Since EPI is unlikely to be sensitive to discrete phase changes from intracortical vein sizes running parallel to the cortical surface [3], this could have blurred BOLD signal changes produced by right and left monocular stimulation. Partial volume effects between adjacent ODCs due to the width of the columns compared to the voxel size could also have been responsible for the inability to separate the responses during right and left monocular stimulation. These results show that the improved spatial specificity of GRE BOLD with phase regression advantageous when performing a laminar analysis, but phase regression struggles to reveal mesoscopic cortical structures.

3.2   Limitations

Studying the human visual cortex poses many additional challenges over other cortical areas. The visual cortex is one of the thinnest parts of the cortex, making laminar and columnar analysis of high-resolution functional data quite difficult. Even with sub-millimeter functional resolutions, which in most current human laminar fMRI studies is limited at approximately 0.75-0.8 mm isotropic [4], there are only about 2-3 voxels across the depth of the visual cortex. This means that the resolution of the functional image is relatively coarse compared to the curvature of the cortex, which increases the amount of partial volume errors during cortical grey matter segmentation. The cortical thickness also varies between sulci and gyri [4], which further increases the difficulty to perform segmentation. In nearly all laminar fMRI studies the data is upsampled, but this does not improve automated cortical segmentations that are performed using most of the available software, as they still produce coarse outlines of the grey matter. At sub-

millimeter resolutions, a coarse cortical segmentation can have a significant effect on the analysis due to partial volume effects and entire voxels that could be in the CSF or WM. To take advantage of the upsampled data, manual correction of grey matter segmentation is often required when performing high-resolution analyses [5]. While this is often necessary, it can introduce significant amounts of error and is very time consuming. Imaging with higher in-plane resolutions helps to reduce the coarseness of the segmentation compared to the curvature of the cortex, but this also reduces the SNR which is compensated by an increased slice thickness. This limits the ability to examine both layers and columns simultaneously, which requires a sub-millimeter resolution in all three dimensions. This remains one of the main difficulties in high-resolution fMRI studies, as it is heavily reliant on MR systems and techniques [5,6] that can provide the required SNR and spatial specificity for sub-millimeter isotropic voxels.

Performing phase regression requires both magnitude and phase data from GRE BOLD. Phase data is not commonly used in fMRI studies and on most MR systems the default coil combination is not optimized for phase reconstruction. This results in the default phase data containing many spatial and temporal wraps. There are unwrapping techniques such as ROMEO [7], which was used in the study in Chapter 2, that can help reduce the number of wraps in the phase data, but the most significant improvements in the phase data come from the use of a phase sensitive coil combination [8]. The necessity of quality phase images makes a phase sensitive coil combination crucial for the performance of phase regression and hinders the simplicity of applying phase regression to GRE BOLD data. For phase regression to become a more commonly used technique it should be paired with a standardized phase sensitive coil combination.

Partial Fourier is not essential for phase regression, but it allows for imaging with higher spatial and temporal resolutions which are important in laminar and columnar analyses [6]. However, partial Fourier has also been shown to cause blurring in high-resolution fMRI [9]. Smoother phase data due to improved phase reconstruction should help reduce the negative consequences of spatial phase blurring, but this could still be a

problem between voxels with and without veins. The difference between the change in the phase angle found in voxels with and without visible veins was shown to be just over 0.1 radians [10]. The blurring effect on the phase data between voxels without veins and voxels with veins needs to be investigate because it could alter the relationship between magnitude and phase data, thus altering the amount of venous suppression.

This study had a small number of participants, which is common in high-resolution laminar fMRI studies. It would be beneficial to increase the number of participants in future studies to verify the statistical relevance of certain parts of this study, such as if preferred eye stimulation consistently produces greater BOLD signal changes with and without phase regression. Since phase regression requires phase data to be saved alongside the magnitude data, this doubles the amount of data that is essential from each scan. Correspondingly, this approximately doubles the time spent on data preprocessing. While this is done offline so it does not affect the scan duration, it still increases the amount of time and memory spent on preprocessing per participant. Preprocessing high-resolution fMRI data is inherently more time consuming as there are increased amounts of voxels, and it often utilizes additional preprocessing steps to aid with SNR, spatial specificity, and accurate cortical segmentations. If phase regression is to be used in a larger study, it will significantly affect the amount of time and memory used before the data can be analyzed.

3.3   Future Directions

Perhaps the biggest advantage of GRE BOLD with phase regression opposed to other imaging sequences that have greater spatial specificity is its higher temporal resolution, which increases the statistical power of the data. The improved spatial specificity that phase regression provides, along with the higher temporal resolution of GRE BOLD allows for the study of local functional connectivity between cortical layers. This technique can push the boundaries of high-resolution fMRI by examining differences between feedforward and feedback processes in V1. Feedforward and feedback processes are associated with inputs and outputs in primary sensory regions, which have been

shown to be separated by cortical layers [11]. Examining feedforward and feedback processes in vivo using local functional connectivity could help further our current knowledge on neural microcircuits in human V1. This is possible because phase regression helps remove the venous bias which has plagued BOLD fMRI studies of functional connectivity across cortical depths.

3.4   Conclusions

Laminar and columnar analyses have been becoming increasingly prominent over the past decade in high-resolution fMRI research, leading to advances in acquisition and analysis techniques. This study expands on previous research involving phase regression at high resolutions by determining its efficacy when performing laminar and columnar analyses in humans. Examining a well-known mesoscopic cortical structure such as ODCs provided a means to assess the results produced with phase regression. This thesis demonstrates that phase regression is an effective technique for removing the large vessel venous bias from the BOLD signal and it is beneficial for improving the spatial specificity of laminar fMRI studies.

3.5   References

[1] R. Turner, How Much Cortex Can a Vein Drain? Downstream Dilution of Activation-Related Cerebral Blood Oxygenation Changes, Neuroimage. 16 (2002) 1062–1067. https://doi.org/10.1006/nimg.2002.1082.

[2] C.A. Olman, S. Inati, D.J. Heeger, The effect of large veins on spatial localization with GE BOLD at 3 T: Displacement, not blurring, Neuroimage. 34 (2007) 1126–1135. https://doi.org/10.1016/j.neuroimage.2006.08.045.

[3] H.M. Duvernoy, S. Delon, J.L. Vannson, Cortical blood vessels of the human brain, Brain Res Bull. 7 (1981) 519–579. https://doi.org/10.1016/0361-9230(81)90007-1.

[4] J. Goense, Y. Bohraus, N.K. Logothetis, fMRI at High Spatial Resolution: Implications for BOLD-Models, Front Comput Neurosc. 10 (2016) 66. https://doi.org/10.3389/fncom.2016.00066.

[5] J.R. Polimeni, V. Renvall, N. Zaretskaya, B. Fischl, Analysis strategies for high-resolution UHF-fMRI data, Neuroimage. 168 (2018) 296–320. https://doi.org/10.1016/j.neuroimage.2017.04.053.

[6] K. Uğurbil, Imaging at ultrahigh magnetic fields: History, challenges, and solutions, Neuroimage. 168 (2018) 7–32. https://doi.org/10.1016/j.neuroimage.2017.07.007.

[7] B. Dymerska, K. Eckstein, B. Bachrata, B. Siow, S. Trattnig, K. Shmueli, S.D. Robinson, Phase unwrapping with a rapid opensource minimum spanning tree algorithm (ROMEO), Magnet Reson Med. 85 (2021) 2294–2308. https://doi.org/10.1002/mrm.28563.

[8] O.W. Stanley, R.S. Menon, L.M. Klassen, Receiver phase alignment using fitted SVD derived sensitivities from routine prescans, Plos One. 16 (2021) e0256700. https://doi.org/10.1371/journal.pone.0256700.

[9] A.T. Vu, K. Jamison, M.F. Glasser, S.M. Smith, T. Coalson, S. Moeller, E.J. Auerbach, K. Uğurbil, E. Yacoub, Tradeoffs in pushing the spatial resolution of fMRI for the 7T Human Connectome Project, Neuroimage. 154 (2017) 23–32. https://doi.org/10.1016/j.neuroimage.2016.11.049.

[10] R.S. Menon, Postacquisition suppression of large-vessel BOLD signals in high-resolution fMRI, Magnet Reson Med. 47 (2002) 1–9. https://doi.org/10.1002/mrm.10041.

[11] R.J. Douglas, K.A.C. Martin, Neuronal Circuits of the Neocortex, Neuroscience. 27 (2004) 419–451. https://doi.org/10.1146/annurev.neuro.27.070203.144152.

Appendices

Appendix A: Human Ethics Approval – Chapter 2

Date: 2 March 2022

To: Ravi Menon

Project ID: 108810

Study Title: High Resolution Functional Magnetic Resonance Imaging of Columnar and Laminar Structures in the Human Cortex

Application Type: Continuing Ethics Review (CER) Form

Review Type: Delegated

Date Approval Issued: 02/Mar/2022

REB Approval Expiry Date: 01/Mar/2023

Dear Ravi Menon,

The Western University Research Ethics Board has reviewed the application. This study, including all currently approved documents, has been re-approved until the expiry date noted above.

REB members involved in the research project do not participate in the review, discussion or decision.

Western University REB operates in compliance with, and is constituted in accordance with, the requirements of the Tri-Council Policy Statement: Ethical Conduct for Research Involving Humans (TCPS 2); the International Conference on Harmonisation Good Clinical Practice Consolidated Guideline (ICH GCP); Part C, Division 5 of the Food and Drug Regulations; Part 4 of the Natural Health Products Regulations; Part 3 of the Medical Devices Regulations and the provisions of the Ontario Personal Health Information Protection Act (PHIPA 2004) and its applicable regulations. The REB is registered with the U.S. Department of Health & Human Services under the IRB registration number IRB 00000940.

Please do not hesitate to contact us if you have any questions.

Sincerely,

The Office of Human Research Ethics

Note: This correspondence includes an electronic signature (validation and approval via an online system that is compliant with all regulations).

Curriculum Vitae

Name:	Brett T. Liem

Post-secondary Education and Degrees:

Acadia University
Wolfville, Nova Scotia, Canada
2016-2020 B.Sc.

The University of Western Ontario
London, Ontario, Canada
2020-2023 M.Sc.

Honours and Awards:

Canada Graduate Scholarships-Master's Award
Natural Sciences and Engineering Research Council of Canada
2021

Academic All-Canadian
U Sports
2016-2022

Golden A Award
Acadia University
Recognizes graduating students who have been identified as being outstanding among their peers during their time at Acadia
2020

Bronze Medal for Physics
Acadia University
Awarded to graduating students with the highest average in a major
2020

Presentations:
Brett Liem, Atena Akbari, Ravi S. Menon. (2022). BOLD Signal Across Cortical Depths using fMRI with Phase Regression. Robarts Research Retreat, London, Ontario, Canada. Poster.

Brett Liem, Ravi S. Menon. (2021). Mapping Functional Connectivity Between Cortical Layers in Ocular Dominance Columns to Understand Feedforward and Feedback Modulations using Phase Regression fMRI. Neuroscience Research Day, Virtual. Oral Presentation.